Network-Lifetime Maximization of Wireless Sensor Networks

HALIL YETGIN, (Student Member, IEEE), KENT TSZ KAN CHEUNG, (Student Member, IEEE), MOHAMMED EL-HAJJAR, (Member, IEEE), AND LAJOS HANZO, (Fellow, IEEE)

School of Electronics and Computer Science, University of Southampton, Southampton SO17 1BJ, U.K.

Corresponding author: L. Hanzo (lh@ecs.soton.ac.uk)

ABSTRACT Network lifetime (NL) maximization techniques have attracted a lot of research attention owing to their importance for extending the duration of the operations in the battery-constrained wireless sensor networks (WSNs). In this paper, we consider a two-stage NL maximization technique conceived for a fully-connected WSN, where the NL is strictly dependent on the source node's (SN) battery level, since we can transmit information generated at the SN to the destination node (DN) via alternative routes, each having a specific route lifetime (RL) value. During the first stage, the RL of the alternative routes spanning from the SN to the DN is evaluated, where the RL is defined as the earliest time, at which a sensor node lying in the route fully drains its battery charge. The second stage involves the summation of these RL values, until the SN's battery is fully depleted, which constitutes the lifetime of the WSN considered. Each alternative route is evaluated using cross-layer optimization of the power allocation, scheduling and routing operations for the sake of NL maximization for a predetermined per-link target signal-to-interference-plus-noise ratio values. Therefore, we propose the optimal but excessive-complexity algorithm, namely, the exhaustive search algorithm (ESA) and a near-optimal single objective genetic algorithm (SOGA) exhibiting a reduced complexity in a fully connected WSN. We demonstrate that in a high-complexity WSN, the SOGA is capable of approaching the ESA's NL within a tiny margin of 3.02% at a 2.56 times reduced complexity. We also show that our NL maximization approach is powerful in terms of prolonging the NL while striking a tradeoff between the NL and the quality of service requirements.

INDEX TERMS WSN, wireless sensor networks, network lifetime, optimization.

NOMENCLATURE

AWGN	Additive White Gaussian Noise
BER	Bit Error Rate
BPSK	Binary Phase-Shift Keying
BTS	Binary Tournament Selection
CC	Convolutional Code
CFEs	Cost Function Evaluations
DN	Destination Node
E2EB	End-to-End BER
ED	Energy Dissipation
ESA	Exhaustive Search Algorithm
IoT	Internet of Things
LNOH	Least Number of Hops
LRBAT	Largest Remaining SN Battery
LTED	Least Total Energy Dissipation
LUT	Look-Up Table
MCSs	Modulation and Coding Schemes
NL	Network Lifetime

QoS	Quality of Service
QPSK	Quadrature Phase Shift Keying
RANR	Random Route Selection
RBAT	Remaining Battery
RL	Route Lifetime
RSSs	Route Selection Schemes
SINR	Signal-to-Interference-plus-Noise Ratio
SN	Source Node
SOGA	Single Objective Genetic Algorithm
SPTS	Spatially Periodic Time Sharing
TDMA	Time-Division Multiple Access
TS	Time Slot
WSNs	Wireless Sensor Networks

I. INTRODUCTION

A wireless sensor network (WSN) is composed of spatially-distributed autonomous devices communicating in a wireless fashion and utilizing sensors in order to gather information

or to detect certain events of significance in the physical and environmental conditions. These sensor devices are capable of simultaneously sensing, processing and communicating, which offers a vast number of compelling applications [1]–[5], such as environmental monitoring, military battlefield observations, logistic management, health monitoring, industrial control and smart world applications. These applications have been designed for accomplishing a specific objective or a desired task. Therefore, there are several design criteria that necessitate careful consideration, as part of the WSN deployment depending on the application requirements and on the objectives to be achieved [1]–[3], [5]. For example, the channel characteristics [6]–[8], network topology [9]–[12], resource limits, interference management [13]–[15], bit error ratio (BER) and other quality of service (QoS) requirements [15] play a significant role in determining the duration of the network's adequate operation, which is termed as the network lifetime (NL). The *lifetime* of a WSN represents the total amount of time, over which the network remains operational and hence supports the application considered [14], [15]. Therefore, the network's lifetime is one of the most important design factors in WSNs, since all the design objectives can only be met, if the network is operational. Explicitly, in this treatise we specifically focused our attention on the network lifetime (NL) as our main design objective and characterized the trade-off between the NL and the BER, with the BER being our salient QoS requirement. Furthermore, we considered the effect of different network sizes in the context of a specific network topology in order to illustrate the implementational complexity of a battery-constrained interference-limited WSN deployment.

The NL is a crucial metric of enabling the network designer to make informed decisions for the sake of maintaining the desired network performance and QoS in WSNs. The NL usually relies on the limited battery capacity of the sensor nodes within the WSN. Moreover, in realistic applications, such as for example in case of sensors embedded into the glaciers for measuring the climate changes, replenishing the battery energy of the sensors and/or replacing the sensors is usually impractical and/or costly. Therefore, the NL is constrained by the battery of the individual sensors in the WSN [1], [2]. Hence, in [14] we proposed an adaptive scheme for striking a compelling trade-off between the attainable transmit rate and the power dissipated. In [15], we examined a fixed-rate system considering the impact of various physical layer parameters on the NL, including the signal processing power dissipated by each sensor. In such scenarios, only the source node (SN) was allowed to generate information, while the rest of the nodes acted as relays aligned in a string-topology for conveying the source data to the sink node, which is also referred to as the destination node (DN). Therefore, the data can only reach the sink node by guaranteeing the connectivity between the SN and the DN in order to maintain a longer NL.

In this paper we consider routing optimization algorithms conceived for maximizing the NL. We invoke a high-complexity exhaustive search algorithm (ESA) for

TABLE 1. List of symbols.

d	Distance between sensors
V	Number of sensors
T	SPTS parameter
n	Slot indicator
$l_{i,j}, n$	Link l spanning from sensor node i to node j, scheduled for TS n
N	Total number of slots in TDMA time frame per link
Act	Desired communication
Int	Interfering communication
m	Path loss exponent
$G_{i,j}$	Channel gain of a link between the transmitter i and receiver j
$P_{l_{i,j},n}$	Transmit power of link l spanning from node i to node j in TS n
$(P_i)_{max}$	Maximum affordable transmit power assigned to sensor node i
Γ_l	SINR of link l
N_0	Noise power at the receiver
γ	Target SINR value
$\mathcal{L}_n$	Set of links in TS n
$BER_{l_{i,j}}$	BER of the link $l_{i,j}$
T_i	Lifetime of node i
T_R	Route lifetime (RL)
$\mathcal{E}_i$	Initial battery capacity of node i
$f_{ED}(x)$	ED function
u_i	A specific sensor operation imposing ED on sensor node i
P_{sp}	Signal processing power
R_V	Total number of distinct and non-looping routes for given V
$(h+1)$	Number of hops
τ	Number of trials per NL
α	Efficiency of the power amplifier
$\aleph_{gen}$	Number of generations
$\aleph_{ind}$	Number of individuals
Pr_c	Probability of crossover
Pr_m	Probability of mutation

quantifying the upper bound on the NL achieved by a reduced-complexity genetic routing algorithm operated in an interference limited WSN. Moreover, since in [14] and [15] a string-topology was considered, here we extend our network topology to a WSN having random uniformly distributed nodes that are fully connected, as described in [16] and [17], so that the routing behavior of the algorithms can be investigated. In the literature, there is a paucity of contributions on NL maximization relying on low-complexity routing optimization in interference limited WSNs, when maintaining

a target QoS for each transmission link and having sensors that are random uniformly distributed. For example, the authors of [13] considered the joint optimal design of the transmit rate and power, while in [18] scheduling and routing was combined for the sake of maximizing the NL in an interference-limited WSN communicating over an additive white Gaussian noise (AWGN) channel. Similarly, Long *et al.* [19] proposed a data gathering scheme that accomplishes several network performance metrics, including the NL maximization and the end-to-end reliability, while guaranteeing the desired QoS. In [20] the aim of the authors was to minimize the ED, which is not the same objective as the maximization of the NL, as discussed in [21]. However, [13], [18] simply considered a rhombus network topology[1] for illustrating the routing behavior of their proposed algorithm. Similarly, the authors of [20] also considered a simplified network topology, where a low-complexity distributed algorithm was developed for minimizing the ED. In [14], we formulated the NL maximization problem as a non-linear optimization problem encompassing the routing, scheduling, as well as the transmission rate and power allocation operations for transmission over both AWGN and Rayleigh block fading channels using the Lagrangian form and the Karush-Kuhn-Tucker (KKT) optimality conditions. However, in [14] we only considered a string topology, where the impact of the routing on the NL cannot be observed. Similarly, in [15] we optimized the NL of a string topology given the lower bound signal-to-interference-plus-noise ratio (SINR) values per link by analyzing the impact of the physical layer parameters along with the signal processing power dissipation on the NL, while operating both in AWGN and Rayleigh block-fading channels.

The authors of [22] proposed a low-complexity near-optimal genetic algorithm for analyzing the joint link scheduling and routing strategies for the sake of maximizing the traffic delivery from a SN to a specific DN within a given delay-deadline in the context of wireless mesh networks (WMNs). By contrast, in [23] a low-complexity genetic algorithm was advocated for jointly optimizing the channel assignment, power control and routing operations for the sake of throughput maximization in cognitive radio based WMNs. Even though both [22] and [23] proposed genetic algorithms for solving complex cross-layer operation problems at a reduced complexity, neither the energy efficiency nor the NL were considered in the context of the low-complexity routing optimization of WSNs.

The authors of [24] and [25] investigated beneficial uplink scheduling and transmit power control techniques for maximizing the NL of battery driven machine to machine (M2M) devices deployed in long-term evolution (LTE) networks, where both an optimal solution as well as a low-complexity suboptimal solution were presented. To elaborate a little further, the suboptimal solution was capable of

accomplishing a near-optimal NL performance at a significantly reduced complexity than the optimal one. In [26]–[28] the authors considered an optimal routing algorithm as well as a reduced-complexity near-optimal routing optimization algorithm designed for maximizing the NL, while guaranteeing the end-to-end delivery-success probability of WSNs. However, they did not take the inter-node interference into account. Similarly, the authors of [29] presented a utility-based nonlinear optimization problem formulation for the sake of NL maximization and proposed a fully distributed routing algorithm for solving the optimization problem, which can of course only provide a near-optimal solution compared to a centralized technique. Nonetheless, the authors of [9] succeeded in conceiving a distributed algorithm for maximizing the NL, which was capable of approaching the performance of the optimal solution at a lower computational complexity. But again, in [9] the impact of the inter-node interference as well as that of the network size was not considered. The authors of [30] proposed a tree-cluster-based data-collection algorithm for WSNs in conjunction with a mobile sink, where the traffic load of the entire network was balanced, since the sink node was able to move around the network for a certain period in order to collect data and avoid the utilization of the same hot-spots in order to prolong the NL. Similarly, in [31] the authors advocated a low-complexity genetic algorithm for achieving both an enhanced coverage and an improved NL for multi-hop mobile WSNs, but their objective function was to minimize the ED, which also improved the NL. However, as discussed in [21], even though energy conservation is beneficial in terms of extending the NL, it has subtle differences with respect to the NL maximization. This difference is mainly due to the network topologies, which is strictly dependent on the type of the applications considered. For example, for the point to point communication of a single source and a single destination, the NL is fully dependent on the SN, assuming that the DN is plugged into the mains power source. Hence, for this specific scenario, minimizing the energy consumption only at the SN is adequate for maximizing the NL. However, in certain topologies minimizing ED of each individual sensor node may not be sufficient for maximizing the NL. Therefore, only minimizing the ED of each node in the network may not be feasible for maximizing the NL. However, the NL may be extended with the aid of an energy minimization approach depending on the applications and the network topology considered. Furthermore, Shi *et al.* in [35] proposed a low-complexity genetic algorithm for jointly optimizing the power control, the scheduling and the routing to maximize the end-to-end throughput in cognitive radio networks. Moreover, Gu *et al.* [33] studied the options for beneficial base station placement for extending the NL based on a specific problem formulation, given the flow routing and energy conservation constraints. Hence, the authors of [33] developed a heuristic algorithm for solving the NL maximization problem at a reduced complexity, but at the cost of a small reduction in NL compared to the

---

[1]A rhombus network topology is a diamond shaped network topology retaining equal length for all four edges.

optimal NL solution. A multi-objective routing optimization approach was proposed in [34] for extending the lifetime of disaster response networks, where a low-complexity genetic algorithm was utilized for analyzing the trade-off between the ED and the packet delivery delay. Similarly, the authors of [36] formulated the maximum-NL routing challenge as a linear programming problem, where the optimal NL was obtained and compared to the near-optimal NL acquired by the proposed routing algorithm. However, the goal in [36] was to only find the specific flow that maximizes the NL relying on the flow conservation constraint. In [37], the authors considered a distributed ED balancing algorithm based on a game-theoretical approach for data gathering and routing in WSNs, where the inter-node interference was not taken into account. Our study shows some similarities with [22] and [35] in terms of the solution approaches applied to the problems considered, but our main objective is the NL maximization in WSNs, while the authors of [35] aimed for maximizing the end-to-end throughput of cognitive radio networks. By contrast, the authors of [22] focused their attention on the computational complexity of the traffic delivery maximization problem. However, compared to [35], our NL maximization algorithm is capable of achieving a longer NL. One interesting NL maximization technique was proposed by Long *et al.* in [38], where the authors aimed for preserving the source location privacy, which in return extended the NL by minimizing the energy consumption in hotspots. A cross-layer mathematical model was proposed in [39] for high data rate applications of WSNs that exceeds the capability of the low-power 802.15.4 radios, where the authors observed significant improvement in the NL by using twin-standard radios (802.15.4 and 802.11) compared to using only 802.15.4 radios. The major NL maximization techniques with reduced-complexity algorithm design are summarized in Table 2. The network model provided in the above contributions mostly considered simplified topologies of low-complexity networks. In this paper, we consider a WSN relying on randomly distributed and fully connected sensor nodes, which exponentially increases the computational complexity required for the network design and optimization with the number of sensor nodes due to the fully connected nature of the WSN. Explicitly, a fully connected WSN is considered, where one sensor can communicate with any other sensor in the network. This paper considers a low-complexity algorithm designed for maximizing the NL, while guaranteeing a specific worst-case end-to-end BER (E2EB), which provides the BER upper bound of the interference limited WSN considered. We also characterize the trade-off between the proposed low-complexity algorithm and its optimal exhaustive search based benchmarker. Moreover, we compare the NL performance of the different WSN scenarios consisting of various numbers of sensors. Note that in the scenarios considered each transmission link has to satisfy a predefined target SINR, which determines the QoS of the WSN. For the sake of clarity, in the rest of the paper we consider the route lifetime (RL) as the lifetime of a single

route spanning from a SN to a DN, which can be considered as a string topology, whereas the NL is defined as the lifetime of a WSN, consisting of many other routes.

This paper focuses on the cross-layer optimization of the power allocation, scheduling and routing operations for the sake of NL maximization for predetermined per-link target SINR values. We propose an optimal algorithm, namely the above-mentioned ESA at a high complexity for high number of nodes and a near-optimal single objective genetic algorithm (SOGA) exhibiting a reduced complexity in fully connected WSNs. The contributions of this paper are summarized as follows.

1) We propose an extended-NL algorithm capable of exploiting alternative routes exhibiting the longest RL for end-to-end transmission in a fully connected WSN, where the aim is to carry the information generated at the SN to the DN, until the SN's battery becomes completely depleted. More explicitly, the addition of the maximum RL computed over the entire range of alternative routes provides us with an extended NL, since the NL is determined by the RL values, until the SN's battery becomes entirely depleted. Therefore, in this paper the NL values are expected to be higher than those in [14] and [15].

2) We optimize the power, the scheduling and the routing for the sake of NL maximization, where we propose the above-mentioned ESA and SOGA algorithms conceived for random network topologies relying on fully connected nodes. Each SN-DN route is passed to an optimization function, namely the so-called dual-simplex function for finding the optimal RL for the corresponding route, where by definition the ESA finds the best route and its RL by searching through all the possible solutions provided by the given number of nodes in the fully connected WSN. On the other hand, the SOGA finds the best solution, given a predetermined number of generations and GA individuals. We show that the SOGA is capable of finding a near-optimal solution at a significantly reduced complexity compared to ESA, specifically when the number of nodes is larger than 7.

3) During the iterations of the ESA and SOGA algorithms, more than one maximum NL value may be returned. Therefore, the selection of the best route is required, where the selection process determines the best SN-DN route for the end-to-end transmission. The selection process also determines the battery drain of the sensors, which has to be updated after each iteration for the forthcoming RL computation relying on the residual battery charges. Hence, we conceive beneficial route selection schemes (RSSs) for finding the specific route with the least total energy dissipation (LTED), the least number of hops (LNOH), the largest remaining SN battery (LRBAT) charge and the random route selection (RANR). For simplicity, we assume that each hop introduces one unit of delay.

TABLE 2. Milestones of NL maximization techniques with reduced-complexity algorithm design.

Year	Authors	Summary
2005	H. Kwon, T. H. Kim, S. Choi and B. G. Lee [26], [27]	An optimal routing algorithm as well as a reduced-complexity near-optimal routing optimization algorithm was designed for maximizing the NL, while guaranteeing the end-to-end delivery-success probability of WSNs.
2006	Y. Cui, Y. Xue and K. Nahrstedt [29]	A utility-based nonlinear optimization problem formulation was conceived for the sake of NL maximization and a fully distributed routing algorithm was proposed for solving the optimization problem, which can only provide a near-optimal solution compared to a centralized technique.
	R. Madan and S. Lall [9]	A distributed algorithm was proposed for maximizing the NL, which was capable of approaching the performance of the optimal solution at a lower computational complexity.
2007	R. Khanna, H. Liu, and H.-H. Chen [31]	A low-complexity genetic algorithm was advocated for achieving both an enhanced coverage and an improved NL for multi-hop mobile WSNs.
2008	C. Hua and T.P. Yum [32]	Routing and data aggregation were jointly optimized in order to maximize the lifetime of the WSN considered using a distributed gradient algorithm.
2013	Y. Gu, M. Pan and W. Li [33]	The options for beneficial base station placement were studied with the objective of extending the NL based on a specific problem formulation given specific flow routing and energy conservation constraints. A heuristic algorithm was proposed for solving the NL maximization problem at a reduced complexity, but at the cost of a small reduction in NL compared to the optimal NL solution.
2014	H. Chenji and R. Stoleru [34]	A multi-objective routing optimization approach was proposed for extending the lifetime of disaster response networks, where a low-complexity genetic algorithm was utilized for analyzing the trade-off between the energy dissipation and the packet delivery delay.
	H. Yetgin, K. Cheung, M. El-Hajjar and L. Hanzo [14]	The NL maximization problem was formulated as a non-linear optimization problem encompassing the routing, scheduling, as well as the transmission rate and power allocation operations for transmission over both AWGN and Rayleigh block fading channels using the Lagrangian form and the Karush-Kuhn-Tucker (KKT) optimality conditions for reduced-complexity.
2015	C. Zhu, S. Wu, G. Han, L. Shu and H.Wu [30]	A tree-cluster-based data-collection algorithm was conceived for WSNs with a mobile sink, where the traffic load of the whole network was balanced, since the sink node was able to move around the network for a certain period in order to collect data and to avoid the utilization of the same hot-spots in order to prolong the NL.
	A. Azari and G. Miao [24], [25]	Beneficial uplink scheduling and transmit power control techniques were investigated for maximizing the NL of battery driven M2M devices deployed in long-term evolution (LTE) networks, where both an optimal solution as well as a low-complexity suboptimal solution were presented.

4) We provide the E2EB as an upper bound on the BER of the interference-limited fully connected WSN using both uncoded binary phase-shift keying (BPSK), as well as 1/2-rate convolutional coded (CC) hard-decoded and soft-decoded quadrature phase shift keying (QPSK) modulation and coding schemes (MCSs) for the proposed RSSs. We will demonstrate that the 1/2-rate CC soft-decoded QPSK MCS has a higher NL than the other MCSs in all scenarios of the ESA and SOGA.

5) We also demonstrate that the RSS-LRBAT and RSS-LTED outperforms other RSSs in terms of their NL, since they are the most NL-aware RSSs. The E2EB of the RSS-LNOH exhibits a slightly better E2EB versus SINR performance, which is due to its reduced bit error accumulation over the associated lower number of hops.

6) Since we assume that the ED of any operation is negligible, compared to the transmit power, introducing an additional sensor into the WSN extends the NL, since this creates more opportunities for relaying the information over alternative routes. We observe that the NL gain achieved by an additional sensor, when for example the 5th sensor enters the WSN having 4 sensors, provides an approximately 5500 extra hours of NL, when the WSN operates at SINR = 10dB.

7) For a network size given by $V = 7$ the computational complexity is similar for both the ESA and SOGA. However, for larger networks the complexity starts to increase exponentially for the ESA, while it is only increased modestly for the SOGA at the cost of a small NL-reduction compared to the optimal NL for WSNs composed of $V > 7$ nodes.

8) The fully connected network model considered can also be applied to any distributed network having more nodes but less distinct routes. We opted for a fully connected WSNs due to the exponentially increased number of the distinct routes, which provides us with a complex network yet tractable even for a low number of nodes to characterize the capability of our SOGA. Therefore, in our scenarios the performance analysis of the SOGA and ESA is based on the total number of distinct routes.

The rest of this paper is organized as follows. Our system model is described in Section II, which is characterized by its network topology, transmission scheme, physical layer, BER and NL. We also provide an example of the interference model and define the integration of the specific MCSs considered into our system model. Then, our problem formulation and the ESA as well as SOGA are presented in Section III, while our experimental results are provided in Section IV. Finally, we summarize our findings in Section VI.

II. SYSTEM MODEL

We consider a fully connected stationary WSN, where the sensors are randomly and uniformly distributed over the sensor field, as illustrated in Fig. 1, which also portrays how the sensor nodes may join the WSN. Once a pending sensor node
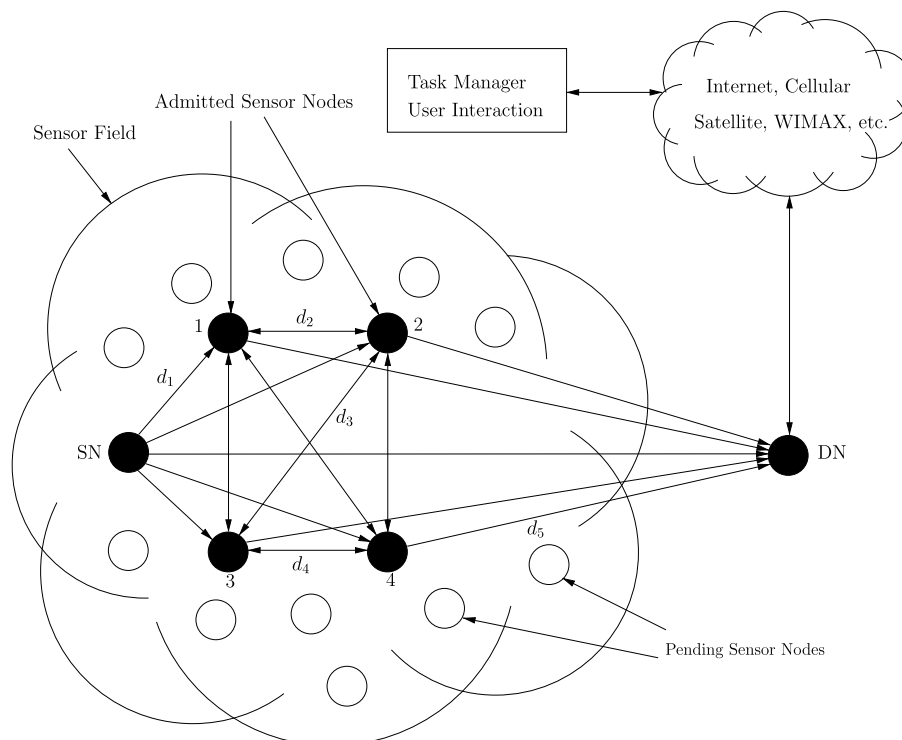

FIGURE 1. Distributed fully connected WSN illustrating the node admission and awaiting sensor nodes.

becomes capable of initiating a communication session with a sensor node in the network, we assume that the pending sensor node can also communicate with any other sensor node in the WSN. Furthermore, we also assume that a sensor node stores the distance information $(d_1, d_2, d_3, \ldots)$ with respect to any other node in the WSN and any changes in the distance information is relayed to the control center, which maintains all the global knowledge concerning the WSN considered at the DN. A communication link can be established between nodes i and j, when node $i \in \{1, \ldots, V\}$, $(i \neq j)$ transmits at its optimum transmit power and node $j \in \{1, \ldots, V\}$ receives a signal with a power higher than a predetermined threshold, where V denotes the number of nodes in the fully connected WSN. We consider a low threshold for guaranteeing that the WSN remains fully connected, as illustrated in Fig. 1, where each sensor is capable of communicating with any other sensor in the network. A fully connected WSN has an exponentially increased complexity upon increasing the number of nodes V. Again, our goal is to study the behavior of our algorithms in a high-complexity fully connected WSN composed of a large number of distinct non-looping routes.[2] Note that the SN and the destination node, which is termed as the DN in the rest of the paper, are located at the opposite corners for ensuring that the geographic distance between the SN and the DN is the longest. The rest of the $(V-2)$ nodes are randomly distributed according to the uniform distribution. Additionally, we assume that only the SN generates information to be transmitted to its neighboring nodes with the aid of a multi hop relaying scheme through to the DN. Therefore, apart from the SN, all nodes in the network act as a relay, which carries information to the DN, as illustrated in Fig. 1. We note that the SN is also capable of directly transmitting to the DN, without the need of a relay node, due to the fully connected nature of the WSN.

Since we assume that only the SN generates information and all the other sensor nodes share a single frequency band, carrying data to the DN requires careful consideration due to the interference. Considering a fully connected network, the SN may have numerous alternative routes for delivering the data to the DN. However, relying on the constrained lifetime of the sensors, choosing the best-lifetime route plays a significant role in keeping the network operational, whilst efficiently utilizing the limited resources of the WSN. Owing to the full connectivity of the WSN, the data generated at the SN can be transmitted until the SN fully drains its battery. We assume that as long as at least one SN-DN route exists in

[2]The term "non-looping route" defines the route with the dissimilar sensor nodes lying in, where one sensor node can only transmit once on the same route, i.e. $SN-1-2-3-DN$ is non-looping, but $SN-1-2-3-1-DN$ is looping, since node-1 repeats in the same route. The term "distinct route" indicates different routes having dissimilar sensor nodes in the same WSN. For example, suppose we can only generate $SN-1-2-3-DN$ and $SN-1-2-3-4-DN$ routes in the same WSN. Then, $SN-1-2-3-DN$ and $SN-1-2-3-4-DN$ are distinct routes, since the second route obtains node-4, which the first route does not have. Therefore, the term "distinct non-looping routes" indicates the routes with non-repeating or dissimilar sensor nodes within the same route and this route differs from another route due to its dissimilar sensor nodes within the same WSN.
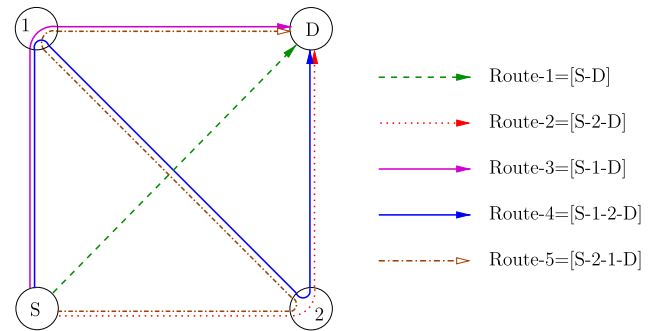

FIGURE 2. A simple WSN having 4 sensor nodes, which exemplifies the RL and NL computation.

the WSN and the battery of the SN is not fully drained, the data transmission from the SN to the DN continues. This process requires the addition of the computed RL values, until the source battery is fully drained. In our system model, at most one SN-DN route can be activated at a time for delivering data to the DN, i.e. we consider a unicast network, and each route is associated with a specific RL value calculated based on the optimization problem to be described in Section III-A. Hence, the maximum RL pair is selected for the transmission of data to the DN. More explicitly, observe in Fig. 2 that there are five distinct non-looping routes, namely Route-1, Route-2, Route-3, Route-4 and Route-5. The term RL refers to the lifetime of any route based on the minimum lifetime of nodes forming part of that particular route, as illustrated in Fig. 2. Additionally, the NL is calculated by the summation of the longest RL values, until the SN's battery is completely drained. For example, we start computing the lifetime of all the routes in the network and assuming that in the first iteration we obtain Route-1=1000 hours (hrs), Route-2=2000hrs, Route-3=3000hrs, Route-4=4000hrs, Route-5=5000hrs of RL values for each of those specific routes. During this iteration, Route-5 will be selected for the end-to-end transmission, since it is the highest RL value computed and hence using that particular route is beneficial for extending the duration of the network's operation. Since our NL model is strictly constrained by the SN's battery energy capacity, we have to check the battery level of the SN after each RL calculation and sum up the longest RL values computed after each iteration. Let us assume for a moment that after the first iteration we still conserved some energy in the SN's battery, therefore the network is still capable of transmitting its information to the DN via alternative routes, which do not rely on the specific sensor node that ran out of battery. Hence, we compute the lifetime of all routes in the current WSN by avoiding the drained sensor node. Let us assume for example that node-1 was the one that completely drained its battery. Then, in the second iteration we assume that we have the following RL values: Route-1=2000hrs and Route-2=4000hrs, which requires Route-2 to be utilized for the next end-to-end transmission. At this stage, if there is no energy left in the SN's battery, then the NL is defined by the summation of the RL values of Route-5 in the first iteration and of Route-2

in the second iteration, which results in $(5000 + 4000 = 9000)$hrs of NL.

A. TRANSMISSION SCHEME

Again, in a fully connected WSN there are numerous alternative routes for the end-to-end transmission. However, selecting the highest-NL route for end-to-end transmission is crucial. Therefore, lifetime of every possible SN-DN route is considered as the RL, which is defined as the time instant at which the first node lying on a given route fully drains its battery. The specific route having the best RL is selected for the final end-to-end transmission, as explained in Fig. 2 of Section II. Moreover, the battery-information of the sensor nodes actually utilized for the end-to-end transmission is updated. After each end-to-end transmission, the battery level of the SN is checked and if the SN battery is not fully depleted, RL computation is updated with the remaining battery power. Here, each maximum RL computation corresponds to one iteration of the algorithm considered. On the other hand, the NL is a function of the RL, until the SN fully depletes its battery. Therefore, the computation of the resultant NL may require a few iterations of the RL computations. Once again, the RL corresponds to the computation of any SN-DN route. Hence, the NL is dependent on the lifetime of the routes of the WSN considered. A unidirectionally communicating route extracted from the omnidirectionally communicating network of Fig. 1 is illustrated in Fig. 3. More explicitly, NL computation relies on the unidirectional links of the available routes extracted from the WSN of Fig. 1, despite the fact that the communication of the WSN is omni-directional. In Fig. 3 the nodes are only capable of transmitting unidirectionally to their consecutive neighboring nodes. We note that a specific SN-DN route of Fig. 3 extracted from the WSN of Fig. 1 can be considered as a single string-topology. Each string-topology extracted from Fig. 1 is utilized for the RL computation by exploiting their distance values, which are correspondingly assigned to the extracted route in Fig. 3, and illustrated as the distances of $(d_1, d_2, d_3, d_4, d_5)$ in Fig. 1.
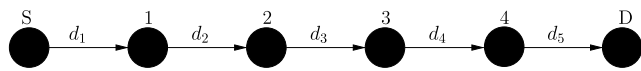

FIGURE 3. A random example of the route extracted from Fig. 1.

The computation of the RL for each extracted route relies on the spatially periodic time sharing (SPTS) technique of [13] for modeling the periodic time slot (TS) activation scheduling used, where we consider a distance of T hops between the pairs of nodes, which are transmitting in the same time TS. The same TSs are reactivated after every T TSs. Fig 4 illustrates the SPTS for $T = 3$, where $[n = 1, n = 2, n = 3, \ldots, n = N]$ describes each TS n for a given N-TS time-division multiple access (TDMA) frame per link and "+" denotes the active links. Therefore, a link l, spanning from node i to node j, scheduled for TS n, is denoted

by $(l_{i,j}, n)$. For example, during the first TS $(n = 1)$, the links $(l_{1,2}, 1)$, $(l_{4,5}, 1)$, $(l_{7,8}, 1)$ are activated for simultaneous transmissions, which only moderately interfere with each other and each link is activated only once during the whole TDMA frame. For the simplicity of our system model, we use $T = 3$ in our SPTS-aided interference-limited scenario and the total number of TSs per link frame is assumed to be $N = 3$ due to its low computational complexity. This means that each link can be scheduled for one of $N = 3$ TSs and in each TS the distance between the scheduled links has to be $T = 3$ hops. We assume that an ongoing transmission is capable of interfering with any other transmission in the extracted route, if they are scheduled during the same TS, as shown in Fig. 5. Naturally, the analysis presented here applies to any arbitrary T value.

For the sake of simplicity, we provide two different illustrations of the same transmission scheme seen in Fig. 3, which allows the reader to readily observe which specific links are activated in a particular TS, giving us a TS-centric view, as illustrated in Fig 5 and which TSs are activated for a particular link, providing us with a link-centric view, as illustrated in Fig. 6. More explicitly, we illustrate the TS-centric view of the SPTS strategy for the route illustrated in Fig. 3 in the context of the topology seen in Fig. 1, where we can observe how many links are activated per TS in Fig 5. Due to the periodic nature of the SPTS for $T = 3$, the third TS $(n = 3)$ contains only a single active link for the 6-node scenario of Fig. 5. If a 7-node route were to be considered, another link would have appeared in the third TS obeying the $T = 3$ scheduling scheme, which can be clearly inferred from the 10-node scenario of Fig. 4.

As a further insight, we provide the link-centric view of the SPTS strategy in Fig. 6, so that we can clearly observe how many times a specific link is activated in each TS. Since this specific scenario is proposed for $N = 3$ TDMA frames and $T = 3$, observe in Fig. 6 each link only has been activated once in different TSs. When the first TS $(n = 1)$ is activated obeying the SPTS of $T = 3$, the links $l_{S,1}$ and $l_{3,4}$ start their actual transmission actions Act_1 and Act_2 over their arbitrary link-distances d_1 and d_4, respectively in Fig. 7. However, during Act_1, node-3 initiates an interfering transmission to node-1 denoted by Int_1. In the mean time, during Act_2, SN concurrently initiates an interfering transmission to node-4, which is denoted by Int_2. Therefore, we can readily see that the interferers (interfering nodes) of the link $l_{S,1}$ and $l_{3,4}$ are node-3 and node-SN, respectively. Since there are only 2 scheduled links in the same TS, one link interferes with another one. If there were 3 links scheduled in the same TS obeying the SPTS of $T = 3$, one link would have been concurrently interfered with the other two. More explicitly, a receiving node would have been exposed to more interference emanating from additional interferers.

B. PHYSICAL LAYER

The sensor nodes of the fully connected WSN rely on using omni-directional antennas. This implies that a SN-DN route
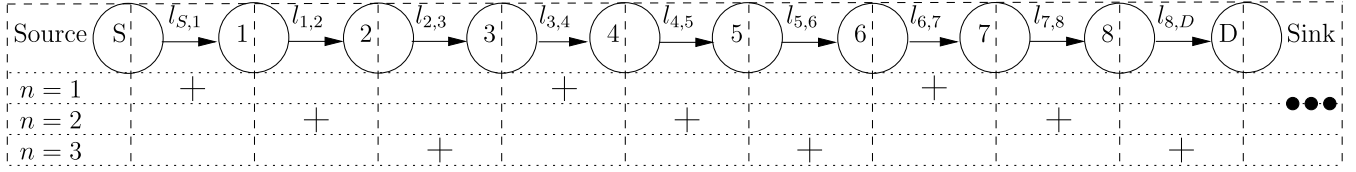
FIGURE 4. SPTS with time sharing parameters of $T = 3$ and $N = 3$ for $V = 10$ nodes.
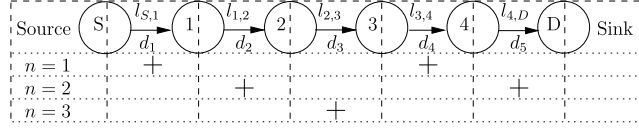

FIGURE 5. TS-centric view of the SPTS for the 6-node route string-topology of Fig. 1, which is illustrated in Fig. 3, when $T = 3$ and $N = 3$.

FIGURE 6. Link-centric view of the SPTS for the 6-node route string-topology of Fig. 1, which is illustrated in Fig. 3, when $T = 3$ and $N = 3$.
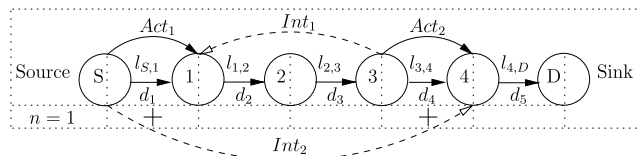

FIGURE 7. Interference model for the extracted 6-node route string-topology of Fig. 1, when $T = 3$.

selection process takes place with the aid of omni-directional communication. Once a route is selected, the communication is handed over to uni-directional links, because information can only flow from a SN to a DN along the selected route. Additionally, the nodes use half-duplex communications, where each node can either transmit or receive in the same TS n. We note that the sensor nodes communicate via the same shared wireless channel. The channel gain of a link between the transmitter i and the receiver j is given by $G_{i,j, i \neq j} = 1/(d_{i,j})^m$, which encapsulates the path loss, where the power diminishes with $d_{i,j}^m$ as a function of the distance $d_{i,j}$

between the transmitter i and receiver j, with the path loss exponent denoted by m. In addition, each node is capable of transmitting at an adjustable transmit power between the no-transmission state and the maximum affordable transmit power assigned to that node, given by $0 \leq P_{l_{i,j}} \leq (P_i)_{max}$. Each node has an initial battery capacity that cannot be exceeded by the total ED of the node.

The AWGN channel is defined by a certain propagation path-loss model and a fixed noise power at the receiver. The link quality is defined in terms of the SINR, which is denoted by Γ_l for the AWGN channel model and it is given by [40]

$$\Gamma_{l_{i,j},n} = \frac{G_{i,j}P_{l_{i,j},n}}{\sum_{i' \neq i, l_{i',j'} \in \mathcal{L}_n} G_{i',j}P_{l_{i',j'},n} + N_0},$$

for a specific link l, where $P_{l_{i,j},n}$ denotes the transmit power of link l spanning from node i to node j in TS n and N_0 is the noise power at the receiver. Note that the SINR of each link in the extracted route cannot be lower than the target SINR γ given by $\Gamma_{l_{i,j},n} \geq \gamma$, $\forall n$, $l_{i,j} \in \mathcal{L}_n$, where $l_{i,j}$ denotes the link between transmitter i and receiver j, while $\mathcal{L}_n$ is the set of links activated in the same TS n. On the other hand, $G_{i',j}$ denotes the channel gain of a link between the interfering node and the receiving node of the desired communication, while $P_{l_{i',j'},n}$ is the transmit power of the interfering link l spanning from node i' to node j' in TS n, where i' is the transmitter and j' is the receiver of the link interfering with the desired communication.

In our system model, we rely on a BER-SINR look-up table (LUT) for characterizing the upper layers, which specifies the particular SINR value to be satisfied for the sake of maintaining a given target BER. Note that we consider the interference to be noise-like in the SINR calculation.[3] Upon knowing the SINR constraint and our deterministic path loss model, we can calculate the interference imposed on the intended receivers, depending on which TS is activated, as shown in Fig. 7, assuming that the actual communication occurs between the SN and node-1 during the first TS. Then, the interference power at the receiving node-1 can be expressed as $Int_1 = G_{3,1}P_{l_{3,4},1} = P_{l_{3,4},1}/(d_2 + d_3)^m$ and the power received at node-1 can be formulated as $Act_1 = G_{S,1}P_{l_{S,1},1} = P_{l_{S,1},1}/(d_1)^m$. Note that if we consider a fixed noise power at the receiver, then we can compute the

---

[3]Since in practice the WSNs rarely encounter a single dominant interferer, the interference is typically constituted by the sum of several interfering components, which allows us to approximate the interference by noise.

SINR of link $l_{S,1}$ during the first TS as in (1),

$$\Gamma_{l_{S,1},1} = \frac{G_{S,1}P_{l_{S,1},1}}{G_{3,1}P_{l_{3,4},1}+N_0} = \frac{P_{l_{S,1},1}}{(d_1)^m} \cdot \frac{(d_2+d_3)^m}{P_{l_{3,4},1}+(d_2+d_3)^m N_0}$$

$$= \left(\frac{d_2+d_3}{d_1}\right)^m \frac{P_{l_{S,1},1}}{P_{l_{3,4},1}+(d_2+d_3)^m N_0} \quad (1)$$

where only a single node interferes with node-1. However, in a scenario, where more than two links are activated during the same TS, we have to sum up the interferences imposed on the corresponding receiver node, along with the fixed noise power. Now Eq. (1) invoked for calculating the SINR of any link in any TS can be generalized for any given route as

$$\Gamma_{l_{i,j},n} = \frac{G_{i,j}P_{l_{i,j},n}}{\sum_{i'\neq i,l_{i',j'}\in\mathcal{L}_n} G_{i',j}P_{l_{i',j'},n}+N_0},$$

which defines the quality of the corresponding link. Therefore, we set $\Gamma_{l_{i,j},n} \geq \gamma$, which can be rewritten as follows,

$$\gamma \cdot \left(\sum_{i'\neq i,l_{i',j'}\in\mathcal{L}_n} G_{i',j}P_{l_{i',j'},n}+N_0\right) - G_{i,j}P_{l_{i,j},n} \leq 0. \quad (2)$$

Let us consider a communication session taking place between node i and j separated by a distance of $d_{i,j}$, where the BER of the link $l_{i,j}$ is denoted by $BER_{l_{i,j}}$. This error probability, plausibly depends on the SINR experienced at the receiver node j of the link $l_{i,j}$, on the modulation scheme, on the channel coding and on the characteristics of the channel. Considering a multi hop scenario, consisting of more than one link, we can derive an expression for the E2EB defined by the BER accumulated along the route spanning from the SN to the DN given by [41], [42],

$$E2EB_{route} = 1 - \prod_{l=1}^{V-1}(1-BER_l), \quad (3)$$

where BER_l is a function of the SINR ($BER_l = f_{MCS}[SINR_l]$), which can be fetched from the LUT selected for the specific MCS employed and $(V-1)$ is the number of links along the *route*. In this contribution, we consider an uncoded BPSK modulated system and a 1/2-rate CC hard-decoded as well as soft-decoded QPSK scheme communicating over an AWGN channel. We can compute the NL of any of the different MCSs by relying on their BER-SINR LUT for the system considered. Note that since we can estimate the BER at the relay nodes, we invoke a decode and forward scheme in our scenarios, where we neglect the ED of the coding and decoding operations. At the DN, all ED is ignored, since we assume that the DN is plugged into the mains power source. The BER-SINR relationship of the system model considered for transmission over the AWGN can be observed in Fig. 8, where for SINRs in excess of 4dB, CC soft QPSK outperforms both CC hard QPSK and uncoded BPSK. Moreover, to guarantee a BER of 10^{-2} or lower, CC soft QPSK requires the lowest SINR, which is the most energy-efficient MCS amongst our MCSs considered. The CC hard QPSK is the
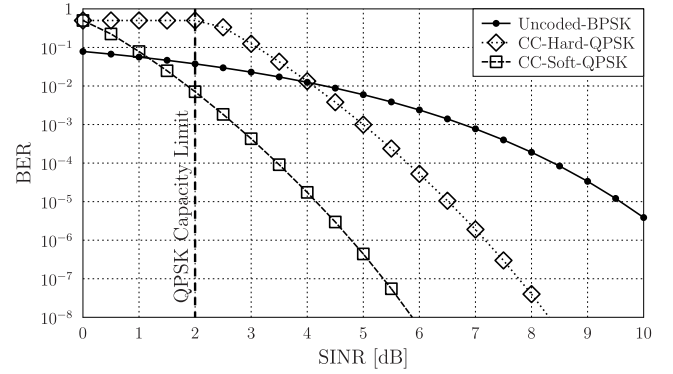

FIGURE 8. BER versus SINR performance of the MCSs considered for an AWGN channel.

second most energy-efficient MCS. Therefore, we also expect to see a similar pattern in terms of the NL for the system model considered, which will indeed be confirmed by the results of Section IV.

C. LIFETIME MODEL
In our model, we consider a novel two-stage lifetime evaluation process, as exemplified by a simplified scenario in Fig. 2 of Section II. The first stage is related to the RL, which is based on the maximization of the minimum node lifetime given by $T_R = \min_{i\neq DN, i\in V} T_i$, where T_i denotes the lifetime of node i lying on the route R. This lifetime definition is realistic, especially if the failure of any node in the route disconnects the SN and the DN. More explicitly, in a route, where the information generated at the SN has to be relayed to the DN via multiple hops, this NL definition is feasible, since a node in the route cannot communicate with the node that is two hops away.

The second stage of the lifetime computation is strictly dependent on the RL computation of the first stage, where each computed maximum RL is summed up, until the SN battery is fully depleted. More explicitly, the best route associated with each maximum RL computation is relied upon for the end-to-end transmission and the sensor nodes lying on those best routes are updated with the remaining battery-levels for the next RL computation. Each maximum RL is summed up in order to calculate the NL, until the SN battery is fully depleted. Since our only concern is that of carrying the SN's information to the DN with the aid of alternative routes, the NL is strictly dependent on the SN's battery level. Therefore, until the SN fully depletes its battery, the maximum RL values are added for calculating the NL in the second stage, as exemplified in Fig. 2 of Section II. Note finally that there are also other alternative NL definitions, which were discussed in [3], [12], [15], and [43]–[45]. In summary, the NL models considered in the literature are as follows.

1) The most commonly used NL model is defined by the earliest time instant at which any of the sensor nodes in the network fully depletes its battery energy.
2) The time instant, until a certain fraction of operational nodes exists in the network.

3) The time, at which the first cluster head fully discharges its battery energy.
4) The time, when all the sensor nodes in the network fully deplete their battery energy.
5) The duration, when the target area is covered by at least k number of nodes, which was termed as the k-coverage.
6) The time, until a specific target area or whole area is covered by at least a single sensor node.
7) The time duration, in which a certain fraction of a region is covered by at least one node.
8) The time duration, in which the coverage falls below a predefined threshold.
9) The total amount of time, until either the coverage or the packet delivery ratio falls below a certain threshold.
10) The time, until a certain amount of information is transmitted.
11) The time, until a percentage of sensors in the network maintains a specific path to the base station.
12) The time, when either the connectivity or the coverage is lost.
13) The duration, until the network becomes incapable of maintaining a reasonable event detection ratio.
14) The duration, until the concurrent analysis of connectivity probability and k-coverage stays above a predefined threshold.
15) In [46], a parameterized NL definition, including the above common definitions, such as node availability, coverage, connectivity, service disruption tolerance and so on, is provided. This NL definition can be used for most of the applications, since the required objective can be incorporated into or discarded from the formulation of the NL definition.

III. PROBLEM FORMULATION

Our NL maximization problem is divided into two stages. The first stage considers the formulation of the system model described in the context of the route extracted, which forms a string topology, followed by the selection of the best RL-aware route. The second stage includes the specific design of the algorithm conceived for maximizing the NL by summing up the RL values, until the SN battery becomes entirely depleted in the WSN considered. We detail the RL computation in Section III-A, followed by the maximum NL computation in Section III-B, where the complexity of a fully connected WSN is also characterized as a function of V. Furthermore, we study the details of both the ESA and SOGA of Section III-B followed by the run-time simulation analysis of both algorithms in Section III-B.

A. ROUTE LIFETIME COMPUTATION

Let us first discuss the problem formulation regarding the routes extracted, which are the SN-DN routes obtained from the fully connected WSN illustrated in Fig. 1, for a given number of nodes per network. Having discussed the system model in Section II, we focused our attention on the general optimization problem formulation for the first stage of maximizing the NL in (4) subject to the constraints of (5)–(7).

$$\max. \ T_R \tag{4}$$

$$\text{s.t. } \Gamma_{l_{i,j},n} \geq \gamma, \ \forall n, l_{i,j} \in \mathcal{L}_n \tag{5}$$

$$\frac{T_R}{N} \sum_{n=1}^{N} \left(\sum_{l \in \mathcal{O}(i) \cap \mathcal{L}_n} \left((1 + (1-\alpha)) \cdot P_{l_{i,j},n} + P_{sp} \right) \right)$$
$$\leq \mathcal{E}_i, \quad \forall i \tag{6}$$

$$0 \preceq P_{l_{i,j},n} \preceq (P_i)_{max}, \quad \forall n, i, l_{i,j} \in \mathcal{L}_n \tag{7}$$

$$\min. \ z \tag{8}$$

$$\text{s.t. } \gamma \left(\sum_{i' \neq i, l_{i',j'} \in \mathcal{L}_n} G_{i',j} P_{l_{i',j'},n} + N_0 \right) - G_{i,j} P_{l_{i,j},n} \leq 0,$$
$$\forall n, \{i : i \in \mathcal{O}^{-1}(l), \ l \in \mathcal{L}_n\}, \tag{9}$$

$$\sum_{n=1}^{N} \left(\sum_{l \in \mathcal{O}(i) \cap \mathcal{L}_n} \left((1 + (1-\alpha)) \cdot P_{l_{i,j},n} + P_{sp} \right) \right)$$
$$- z \cdot \mathcal{E}_i \cdot N \leq 0, \ \forall i, \tag{10}$$

$$0 \leq P_{l_{i,j},n} \leq (P_i)_{max}, \ \forall n, i, l_{i,j} \in \mathcal{L}_n. \tag{11}$$

We maximize T_R in (4) in order to maximize the minimum lifetime of nodes lying on the route extracted, while obeying the constraints mentioned in our system model. For example, (2) formulates the link quality, given the relationship between the attainable rate, the signal power and the interference imposed as well as the noise power encountered at the receiver, which can be associated with the QoS. Therefore, (5) may be formulated as a constraint to be satisfied for guaranteeing the QoS at a specific predetermined target SINR value. Additionally, each sensor node relies on limited batteries, which cannot be replenished. Therefore, the ED of a single sensor cannot exceed its initial battery charge level $\mathcal{E}_i$, which can be readily written as $\sum_{u_i}^{U} f_{ED}(x_{u_i}) \leq \mathcal{E}_i$, where $u_i = \{1, \ldots, U\}$ characterizes the sensor operations imposing a specific ED and $f_{ED}(x)$ is the ED function. We assume that any operation other than the transmission of information across the network incurs a negligible ED. Therefore, the signal processing power dissipation P_{sp} is set to 0 and u_i can be set to 1, since the transmit power is the only reason for dissipating energy in the sensor. Then, $f_{ED}(x)$ can be characterized by (6), representing how the initial battery energy is dissipated as a function of both the system parameters and of the transmit power $P_{l_{i,j}}$, where α denotes the power amplifier's efficiency and N corresponds to the total number of TSs per link, $n = \{1, \ldots, N\}$.

For simplicity, in our scenarios we consider $N = 3$. For example, for the topology defined in Fig. 5, links $l_{S,1}$ and $l_{3,4}$ are activated in the first TS ($n = 1$), links $l_{1,2}$ and $l_{4,D}$ are activated in the second TS ($n = 2$), and link $l_{2,3}$ is activated in the third TS ($n = 3$). Moreover, (7) indicates that the transmit power can be adjusted to the no-transmission state of $P_{l_{i,j}} = 0$ or to the maximum affordable transmit power at any sensor $P_{l_{i,j}} = (P_i)_{max}$ or to any value between 0 and $(P_i)_{max}$, depending on the SPTS parameter of $T = 3$ and on the

other optimization variables. Explicitly, the variables of the optimization problem are the RL T_R and the transmit power $P_{l_{i,j},n}$ of the link spanning from sensor node i to node j in TS n. It is clear that (4)–(7) is non-convex owing to their reliance of the product of two optimization variables, which is generally non-convex [47].

We can readily transform the non-convex[4] NL maximization problem into a convex[5] one by minimizing the reciprocal of the RL, which is formulated as $z = \frac{1}{T_R}$ in (8) by using a change of variable in order to avoid the product of the two variables. In fact, the optimization problem is converted into a linear programming problem, which is also a special case of convex optimization problems. Note that T_R cannot be zero in the reciprocal domain, since the SN has a battery capacity of $\mathcal{E}_i > 0$ and a positive lifetime, implying that the SN definitely transmits information for a non-zero amount of time. This is also applicable to any other sensor nodes in the WSN considered. Additionally, Eq. (5) is rearranged into (9). Most importantly, the optimization variables contained in the product are appropriately separated so that (6) becomes linear in (10), which is a special case of convex problems, where $l \in \mathcal{O}(i)$ represents the transmit link of node i. Furthermore, $\{i : i \in \mathcal{O}^{-1}(l), l \in \mathcal{L}_n\}$ in (9) represents the set of nodes, which the transmit links are connected to and that are activated in the same TS.

We compute the maximum RL of the routes obtained from the fully connected WSN using the dual simplex method of the CPLEX library [48], which is a powerful solution method conceived for linear programming problems, as a special case of convex problems. Therefore, the first phase of the NL maximization problem is based on the computation of the RL and on the selection of the best RL-aware route. Generally speaking, based on the transmission scheme proposed in Section II-A, we maximize the NL of an arbitrarily created and uniformly distributed WSN composed of V nodes, where the SN and the DN have their positions fixed at the opposite corners of the sensor field, while the nodes lying on a route adjust their transmit powers for a predetermined target SINR γ for guaranteeing at least the minimum signal quality required for each link, until the NL of the WSN is exhausted due to the depleted SN battery.

B. MAXIMUM NETWORK LIFETIME

In this section, we propose a pair of algorithms for maximizing the NL of our fully connected WSNs. The first technique considered is the so-called exhaustive search algorithm (ESA), which searches for all the possible distinct routes in the given network. The second algorithm, which we refer to as the single-objective genetic algorithm (SOGA), intelligently searches through a fraction of the potentially excessive solution space for finding the optimum at a low

---

[4]Non-convex optimization problems may have local optimal points. However, these local optimal points mostly will not be the global optimal solutions. Additionally, proving that there is no feasible solution can be time consuming and is not guaranteed.

[5]Convex optimization problems can only have one global optimal solution and one can easily prove if there is no feasible solution to the convex problem.
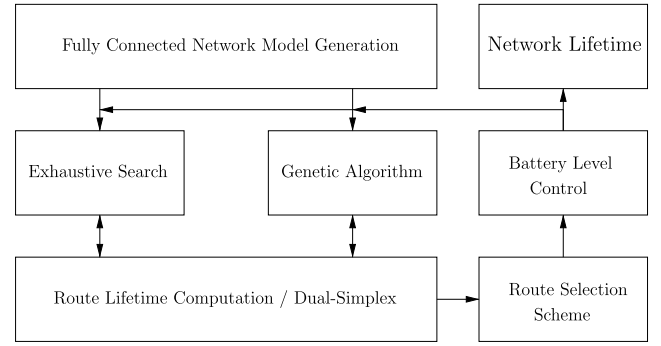

FIGURE 9. A single trial of the general NL computation framework for ESA and GA.

complexity. The general structure of our algorithms can be seen in Fig. 9, where each algorithm starts with a fully connected network-creation. Then, beneficial route discovery and route evaluation processes are provided by the proposed algorithms. The route information obtained is utilized for RL computation for each route selection scheme. Since the NL is strictly dependent on the SN, the battery level of the SN is updated by both algorithms. Having a large number of nodes in a fully connected network leads to an exponential increase of the number of routes, which imposes an exponentially increasing complexity. Therefore, we first provide the complexity analysis of the fully connected network before describing our proposed algorithms.

1) FULLY CONNECTED WSN AND COMPLEXITY ANALYSIS

Short-range densely deployed sensor networks can be used for numerous realistic applications [1], [2], where any sensor between the SN and DN may act as a relay to forward the information of the SN. For example, in battle fields non-rechargeable sensors can be densely deployed for maintaining the lowest battery consumption and for keeping the network operative as long as possible. Another example of densely deployed short-range networks can be found in a football stadium, where each person carries a sensor for health and security reasons. Finally, earth quake monitoring requires a dense sensor deployment for measuring the backscattered wave fields [49]. Therefore, all of these applications may necessitate communication of a node with any other node in the network, which leads to a fully connected WSN. More explicitly, a WSN associated with numerous communication links can be represented by a tractable fully connected WSN. However, the complexity is an important issue in fully connected networks, since the number of distinct non-looping routes increases exponentially upon increasing V. The term "distinct non-looping routes" indicates the routes associated with distinct sensor nodes within the same route and this route differs from any other route due to its unique sensor nodes within the same WSN. The total number of distinct and non-looping routes is given by

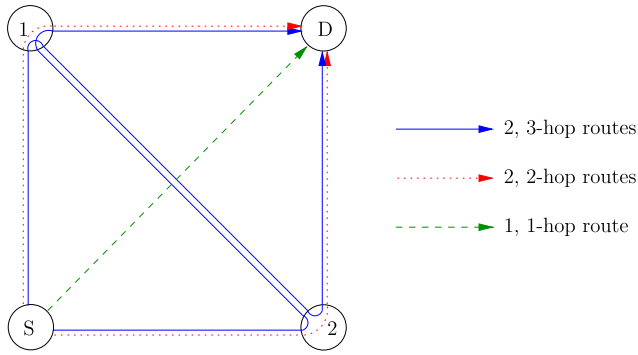$$R_V = \sum_{h=0}^{V-2} \frac{(V-2)!}{(V-2-h)!}, \qquad (12)$$

FIGURE 10. An example of distinct route permutations for a 4-node fully connected WSN.

which is basically the aggregation of all the route permutations for each route having $(h+1)$ links or hops, given the total number of V nodes in the network. As an example, we provide the route permutations of a 4-node fully connected WSN in Fig. 10, where Eq. (12) constructed for a scenario associated with $V = 4$ leads to:

$$R_{V=4} = \sum_{h=0}^{4-2} \frac{(4-2)}{(4-2-h)} = \sum_{h=0}^{2} \frac{2!}{(2-h)!}$$
$$= \frac{2}{(2-0)!} + \frac{2}{(2-1)!} + \frac{2}{(2-2)!}$$
$$= 1 + 2 + 2 = 5, \tag{13}$$

which can also be verified with the aid of Fig. 10. It is clear from the equation that the permutation is calculated in a hop-by-hop manner. We know that the values of 0, 1 and 2 are denoted by h in the denominator of $\frac{2}{(2-0)!}$, $\frac{2}{(2-1)!}$, $\frac{2}{(2-2)!}$ and $(h + 1)$, i.e. 1, 2 and 3, represents the number of hops. Therefore, Eqs. (12) and (13) indicate that $\{1, 2, 2\}$ number of distinct route permutations are calculated for the corresponding number of hops $\{1, 2, 3\}$, respectively. This can also be confirmed using Fig. 10, which is illustrated by the blue solid lines for the 3-hop, by the red dotted lines for the 2-hop, by the green dashed line for the 1-hop communication scenarios, respectively. It is observed that there are two 3-hop, two 2-hop and one 1-hop distinct routes, which is summed up to 5, as seen in Eq. (13) using Fig. 10. Naturally, we can also say that any route constructed for a given network can have a maximum of $(V - 1)$ hops starting from 1-hop communication.

We provide Table 3 for V nodes as a reference for evaluating the associated complexity trade-offs, representing how the total number of distinct non-looping routes changes as a function of the number of nodes using (12). Table 3 also portrays that the complexity increases exponentially as a function of V. Since we quantify the complexity of the algorithms in terms of the total number of function calls to the RL evaluation, i.e. by the number of cost function evaluations (CFEs), the complexity is linearly proportional to the number of distinct non-looping routes.

TABLE 3. Total number of distinct non-looping routes as a function of V.

V	Number of distinct non-looping routes
3	2
4	5
5	16
6	65
7	326
8	$1,957$
9	$13,700$
10	$109,601$
15	1.6927×10^{10}
20	1.7403×10^{16}

2) EXHAUSTIVE SEARCH ALGORITHM

Algorithm 1 shows the exhaustive search algorithm (ESA) used for maximizing the NL, which can be summarized as follows.

We initialize the parameters in the "input" section of Algorithm 1 for V, such as the target SINR γ, number of trials τ and the initial battery capacity $\mathcal{E}_i$ of each sensor. Note that the SN is always considered to be the first node and the DN is always set as the last node. Let us assume that a fully connected WSN is composed of 10 sensor nodes. Then the SN has the unique identifier of 0, while the DN has the unique index of 9.

Then, a fully connected network conceived for a given number of V nodes is created at line 3 of Algorithm 1. We consider a single SN, which is fixed at a coordinate of $(0, 0)$, and a single DN is located at the coordinate of (x_{max}, y_{max}), where $(x_{max} \times y_{max})$m^2 describes the size of the sensor field, guaranteeing that SN and DN are far apart having the longest distance in between. All the other sensors are stationary and randomly distributed according to a uniform distribution. Therefore, the distance of a node from any other node in the network can be readily recorded with the aid of a distance matrix. This scenario may correspond to a network illustrated in Fig. 1, where the Euclidean distance between the SN and the DN is given by $d_{S,D} = \sqrt{(x_{max})^2 + (y_{max})^2}$, which coincides with the diagonal of the sensor field. We rely on the same distance matrix, until we compute the accumulated NL. More explicitly, since the WSN considered is stationary, once the network is created, the distances of all sensors are fixed for a given NL computation.

The SN can transmit the information to the DN along with all possible distinct routes given by Eq. (12). Therefore, all possible SN-DN routes, which can be seen from Table 3 for V number of nodes, are passed on to an optimization function, one at a time. On line 8, the optimization function, namely the so-called dual-simplex, computes the

---

Algorithm 1 ESA for Maximizing the NL Based on the Battery Level of the SN

Input: γ (target SINR)

           τ (number of trials)

           $\mathcal{E}_{init}$ (initial battery of each sensor in the WSN)

           V (number of nodes)

           $(x_{max} \times y_{max})\mathrm{m}^2$ (size of the sensor field starting from $(0, 0)$ to (x_{max}, y_{max}))

           κ (total number of RSS, while i indicates each of the RSS)

           T_{net} (network lifetime)

1: **for** i from 0 **until** κ **do**
2:    **for** j from 1 **until** τ **do**
3:       Create a fully connected, randomly and uniformly distributed network for V
4:       $d_{all} \leftarrow$ Get distance matrix using coordinates of sensors lying on $(x_{max} \times y_{max})\mathrm{m}^2$
5:       $T_{net} = 0 \leftarrow$ Set initial value of NL to zero per created network
6:       $\mathbf{R} \leftarrow$ Discover all possible non-looping routes using (12)
7:       **function** ESA($\mathcal{E}_{init}$, T_{net}, γ)
8:       dual-simplex($\mathbf{R}$, d_{all}, $\mathcal{E}_{init}$, γ) $\rightarrow$ Pass $\mathbf{R}$ to the dual-simplex function
9:       **if** *infeasible*
10:          **eliminate** $\mathbf{R}_{infeasible}$
11:        **else**
12:          $\mathbf{T_R} \leftarrow$ Return the route lifetime of $\mathbf{R}$
13:          $\mathbf{E_R} \leftarrow$ Return the energy usage per node of $\mathbf{R}$
14:          $\mathbf{P_R} \leftarrow$ Return the transmit power per link of $\mathbf{R}$
15:        **end if**
16:       $T_R \leftarrow$ Obtain maximum $\mathbf{T_R}$
17:       $R_{best} \leftarrow$ Reserve the best RL aware routes with T_R
18:       **do while** $\mathcal{E}_{SN} > 0 \leftarrow$ NL strictly depends on the SN battery level
19:          $T_{net} = T_{net} + T_R \leftarrow$ Accumulate each RL value for building the NL
20:          $R_{best} \leftarrow$ Select the best route using RSS$_i$ from $\mathbf{R}_{best}$ for end-to-end transmission
21:          $\mathbf{R}_{final} \leftarrow$ Copy R_{best} to a final array for each iteration of RL.
22:          Update the batteries of all sensors with $E_{R_{best}}$ to obtain $\mathcal{E}_{residual}$
23:          **return** ESA($\mathcal{E}_{residual}$, T_{net}, γ)
24:        **end do**
25:       **return** each T_{net} to an array for averaging NL τ times for given RSS$_i$
26:       $h_{\mathbf{R}_{final}} \leftarrow$ size($\mathbf{R}_{final}$) Gather the hop length of each final route
27:       SINR$_{link} \leftarrow$ Compute SINR of each link using (9) of γ for $\mathbf{R}_{final}$ with $\mathbf{P}_{\mathbf{R}_{final}}$
28:       BER$_{link} \leftarrow$ Obtain BER$_{link}$ of SINR$_{link}$ with the aid of LUT for considered MCSs
29:       E2EB$_{\mathbf{R}_{final}} \leftarrow$ Compute E2EB of each final route using (3) of BER$_{link}$ with $h_{\mathbf{R}_{final}}$
30:       E2EB$_{worst-case} \leftarrow$ Attain the highest E2EB of $\mathbf{R}_{final}$
31:       **return** each E2EB$_{worst-case}$ to an array for averaging E2EB τ times for given RSS$_i$
32:    **end for**
33: **end for**
34: **return** averaged T_{net} and worst case E2EB over τ trials for each RSS

RL according to (8)–(11). Each route associated with a different number of hops in the fully connected network is automatically and appropriately arranged according to it scheduling matrix for RL computation. For example, the active links are determined for each TS n corresponding to the SPTS parameter T, discussed in Section II-A, so that we are capable of identifying the interfering nodes and their gain matrices $G_{i,j}$ in the same TS to compute the interference terms, as shown in (1). Since our objective is to maximize the RL for all possible routes identified by the ESA, each optimization function call returns a RL value as its output, as indicated

in Algorithm 1 on line 12. This implies that we obtain RL values for all the distinct routes in the fully connected WSN considered.

Then, we choose the route associated with the highest RL on line 17. Additionally, since there may be more than one route having the same maximum RL value, we have introduced the RSSs. Four different RSSs are introduced for their appropriate employment in different application scenarios. The first one is based on the total energy usage of the routes having the maximum RL. We basically select the specific route having the least total ED. In the second RSS, the route

associated with the least number of hops is chosen, since here we assume that each sensor incurs a delay of a single time unit due to queuing delays both at the SN and intermediate nodes. The third RSS relies on the SN battery level. The route associated with the largest remaining SN battery is selected. The last RSS is based on a random route selection strategy. A random route is selected amongst all the routes having the maximum RL value. Note that the selection process exclusively relies on the specific routes having the maximum RL value. Therefore, we expect the NL results of these various RSSs to be similar, which will indeed be confirmed in Section IV. For each of the RSS, we run τ number of trials for averaging the NL results, as indicated on line 25 of Algorithm 1. Moreover, for convenience we term the four route selection schemes mentioned above as RSS-LTED, RSS-LNOH, RSS-LRBAT and RSS-RANR, respectively.

The best selected RL route, based on its RSS, is used for the end-to-end transmission as indicated on line 20 of Algorithm 1. Let us refer to this end-to-end transmission as the "transmission phase". Therefore, a single evaluation of the best RL-aware route indicates that a transmission phase will take place over the reference route, which is the best RL-aware route. During the transmission phase, the battery level of the sensor nodes utilized during this transmission is reduced. Therefore, on line 22 of Algorithm 1, those battery levels have to be updated relying on their appropriately adjusted transmit power conforming to (8)–(11), respectively. Since we consider a scenario, where the NL is strictly dependent on the SN battery level considered on line 18 of Algorithm 1, the SN battery level has to be checked after every transmission phase. If the SN battery is not fully depleted, the ESA continues searching for the next best RL-aware route in the fully connected WSN with its residual (updated) batteries, commencing from the previous transmission phase. Basically, if there is sufficient battery charge at the SN, Algorithm 1 recursively searches for the next best route in the next iteration on line 23. If the SN battery is fully depleted, then the NL is determined by the summation of the maximum RL values gleaned from the previous iterative transmission phases, as indicated on line 19 of Algorithm 1. Note that each NL computation may require a few iterations of the RL-aware route computation or transmission phase, depending on the SN battery status after each iterative transmission phase.

Since we know what the best RL-aware routes are from the various iterations of this specific transmission phase, on line 29 of Algorithm 1 we can invoke (3) for the E2EB calculation of the best RL-aware routes. Note that we assume the best RL-aware routes are indeed reserved by the SN after each transmission phase, as indicated on line 20 and 21 of Algorithm 1. We aim for finding the highest E2EB in the network to determine the upper bound of the BER in our WSN. Therefore, the route associated with the largest E2EB amongst the best RL routes is utilized on line 30 of Algorithm 1. More explicitly, the best RL-aware routes possibly carry the highest E2EB, because these routes are the most power-efficient routes, since the only objective of the optimization problem is to maximize the NL, while maintaining a required QoS. Therefore, finding the highest E2EB amongst these best RL-aware routes is adequate for determining the upper bound of the E2EB in the WSN considered. Additionally, Eq. (9) guarantees maintaining the required signal quality of each link, which has to maintain the predefined target SINR. However, in our results we will confirm that each link attains the exact target SINR values, so that the transmit power per link can be minimized. Minimizing the transmit power can only be achieved by keeping the SINR per link as close as possible to the target SINR, which is given by the Eq. (9) and shown on line 27 of Algorithm 1. Therefore, it is demonstrated on line 28 of Algorithm 1 that the BER per link can be obtained from the LUT of the corresponding SINR, which can then be utilized for the E2EB computation using (3). Therefore, we conclude that for a given MCS and for a specific target SINR per link, the E2EB can be readily determined using (3) along the best RL routes and the route associated with the largest E2EB is used as the upper bound of the BER for the WSN considered, which describes the worst-case E2EB performance of the network, as indicated on line 30 of Algorithm 1.

3) RUN-TIME EXAMPLE OF THE ESA

We consider a 6-node fully connected network, where the SN has the unique identifier of 0 and the DN has the unique index of 5. In order to exemplify the NL computation, we select a target SINR of $\gamma = 0$ dB, where the discrete-input continuous output memoryless channel (DCMC) [50] capacity of QPSK is about 0.5 bit/symbol. The battery capacity per sensor is initialized to 5000 Joule. This simulation example only covers a single trial[6] ($\tau = 1$) of the NL computation for a path loss exponent of $m = 3$ and for the system model considered in Section II.

The size of the sensor field is given by $40 \times 40 m^2$, where the sensors are randomly and uniformly deployed over the sensor field. However, the SN is fixed at a coordinate of $(0, 0)$, while the DN is placed at the other corner of the sensor field associated with the coordinate of $(40, 40)$. Therefore, the distance between the SN and the DN corresponds to the largest possible distance in the network, which is approximately $d_{SN,DN} \approx 56.57$m, as illustrated in Fig. 11.

We can readily observe from Table 3 that the SN has 65 alternative routes for transmitting its data to the DN for $V = 6$. Therefore, the ESA looks for all those possible routes and computes their RL by passing the route information to the optimization function. For this specific scenario, the symmetric distance matrix of the fully connected WSN seen in Fig. 11 can be exported, as observed in Table 4, where we can look up all the distance information of any relevant sensor node. For the sake of clarity, we present the distance conversion matrix of a single actual route $R_{act} = [0 - 4 - 1 - 2 - 3 - 5]$ out of the 65 possible routes.

---

[6]A NL computation *trial* may be constituted by several RL computation *iterations*.
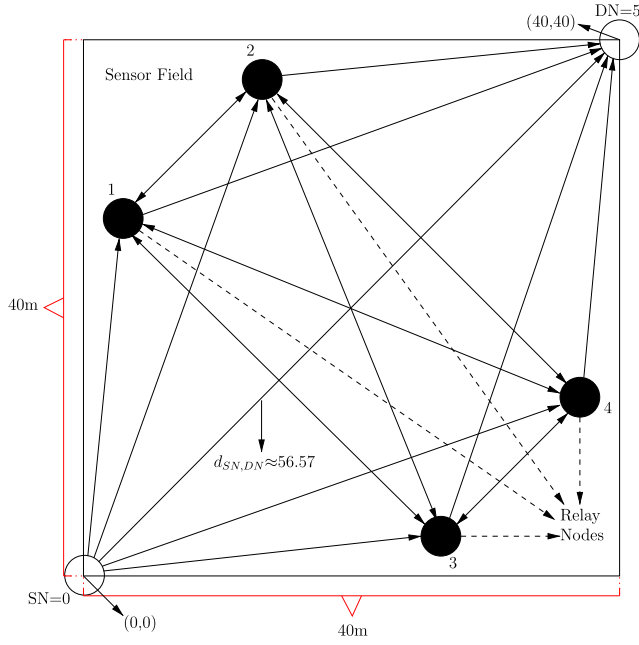
FIGURE 11. Example of a fully connected WSN consisting of 6 nodes (not to scale).

TABLE 4. Distance matrix $d_{i,j}$ of a 6-node fully connected WSN.

nodes $i \setminus j$	0	1	2	3	4	5
0	0	9.03	41.87	42.15	23.64	56.57
1	9.03	0	33.21	33.23	18.38	47.54
2	41.87	33.21	0	4.77	36.12	19.82
3	42.15	33.23	4.77	0	33.67	16.41
4	23.64	18.38	36.12	33.67	0	42.73
5	56.57	47.54	19.82	16.41	42.73	0

TABLE 5. Distance matrix d_{act} of R_{act} including the distance information of the interferers extracted from $d_{i,j}$.

nodes $i \setminus j$	0	4	1	2	3	5
0	0	23.64	0	0	42.15	0
4	23.64	0	18.38	36.12	0	42.73
1	0	18.38	0	33.21	33.23	0
2	0	36.12	33.21	0	4.77	0
3	42.15	0	33.23	4.77	0	16.41
5	0	42.73	0	0	16.41	0

TABLE 6. Distance matrix d_{ord} of R_{ord}, including the distance information of interferers converted from d_{act} using distance conversion matrix.

nodes $i \setminus j$	0	1	2	3	4	5
0	0	23.64	0	0	42.15	0
1	23.64	0	18.38	36.12	0	42.73
2	0	18.38	0	33.21	33.23	0
3	0	36.12	33.21	0	4.77	0
4	42.15	0	33.23	4.77	0	16.41
5	0	42.73	0	0	16.41	0

For the sake of computing the RL in dual-simplex optimization function, arranging the corresponding matrix elements of the distance and $G_{i,j}$ of the WSN is one of the challenging parts of the problem due to the presence of the interference terms. Therefore, in our approach we utilize the distance conversion matrix, where each sensor along the route having a unique identifier is reordered. Let us clarify this with the aid of an example by referencing it to the original distance matrix of Table 4. Firstly, a distance matrix is extracted from Table 4, which is only specified for the route R_{act}. In the mean time, the actual route R_{act} associated with the actual distance matrix d_{act} in Table 5 is converted to the ordered route $R_{ord} = [0-1-2-3-4-5]$ having the distance d_{ord} in Table 6. This approach provides us with the converted route R_{ord} along with the actual distance matrix d_{act} of the route R_{act}. The ordered route R_{ord} exploits the simplified indices of the corresponding sensors, while reserving the required distance values of the actual route R_{act}.

Basically, each time when a route R_{act} is passed to the optimization function, its distance information is assigned to the converted route R_{ord}. Note that the reordered routes can be in the range of $\{0 - 1, 0 - 1 - 2, 0 - 1 - 2 - 3, \ldots, 0 - 1 - 2 - 3 - 4 - 5 - 6 - 7, \ldots\}$, depending on the size of the actual route R_{act}. Additionally, a zero is placed in Table 5 and Table 6, if there are no direct communication links between the nodes lying on the route.

Then, we estimate the gain matrix seen in Table 7 of the reordered route using the distance matrix of Table 6, which is calculated using $G_{i,j} = 1/d_{i,j}^m$, as discussed in Section II-B. Given the gain matrix of Table 7 and using an optimization tool, referred to as the dual simplex function of the CPLEX library [48], we obtain the optimal values of the transmit power and the RL variables.

4) NL COMPUTATION AND BATTERY STATE UPDATE

In the first step of the NL computation, the ESA searches for the best RL-aware routes. For the 6-node fully connected scenario of Fig. 11, ESA finds four different routes having the same maximum RL. These four routes of Fig. 11 are $[0 - 1 - 2 - 5]$, $[0 - 1 - 2 - 3 - 5]$, $[0 - 4 - 1 - 2 - 5]$, $[0 - 4 - 1 - 2 - 3 - 5]$ with a RL of 81,292.4 hours (hrs) for a predefined target SINR value of $\gamma = 0$ dB, as evaluated by the optimization tool. To further elaborate on this specific example, we consider

TABLE 7. Gain matrix $G_{i,j}$ of the route R_{ord}, which is transformed from R_{act}.

nodes $i \setminus j$	0	1	2	3	4	5
0	∞	7.56×10^{-5}	∞	∞	1.33×10^{-5}	∞
1	7.56×10^{-5}	∞	1.61×10^{-4}	2.12×10^{-5}	∞	1.28×10^{-5}
2	∞	1.61×10^{-4}	∞	2.73×10^{-5}	2.72×10^{-5}	∞
3	∞	2.12×10^{-5}	2.73×10^{-5}	∞	9.21×10^{-3}	∞
4	1.33×10^{-5}	∞	2.72×10^{-5}	9.21×10^{-3}	∞	2.26×10^{-4}
5	∞	1.28×10^{-5}	∞	∞	2.26×10^{-4}	∞

a target SINR value of $\gamma = 0$ dB.[7] However, this can be extended for any of the target SINR values of $\gamma = \{0, 0.5, 1, 1.5, \ldots, 9, 9.5, 10\}$ dB. In Section III-B2, we introduced four RSSs to deal with the route selection process, which we referred to as RSS-LTED, RSS-LNOH, RSS-LRBAT and RSS-RANR. However, for this specific example we will only consider RSS-LTED, which reserves the route associated with the least total ED. Therefore, we can identify the best RL-aware route by checking the total ED of each route.

From Table 8, we can observe 3 iterations (iters) of the RL computation, which constitutes one trial NL computation for the $V = 6$-node fully connected WSN. Each iteration of the RL computation evaluates how much of the SN battery (initialized to 5000J) has been dissipated by the route that is selected as the best RL-aware route after each iteration. For example, route $[0 - 1 - 2 - 3 - 5]$ is selected with the aid of RSS-LTED, since it consumes a total of 5733.57J energy, which is the least amount of ED among all the routes.

[7]We compute the NL for the target SINR values of $\gamma = \{0, 0.5, 1, 1.5, \ldots, 9, 9.5, 10\}$ dB. However, as an example here we use only 0 dB SINR to present the routing information, the remaining battery charge and other related operations during the NL computation. We note that for a target SINR value of 0dB, the discrete-input continuous output memoryless channel (DCMC) [50] capacity of QPSK is about 0.5 bit/symbol.

Moreover, since the NL is strictly dependent on the level of the SN battery, the remaining battery (RBAT) of the SN after each iteration of the RL computation is provided in Table 8. During the first iteration, 112.699J of energy is utilized at the SN, while in the second iteration, an amount of 1731.86J is depleted from the SN, which had an instantaneous RBAT of 4887.3J. The RBAT of the SN is reduced to 3155.44J. Finally, in the third iteration an amount of 3155.44J energy is consumed from the RBAT of 3155.44J. Since there is no more energy left in the SN battery, the information cannot be generated and transmitted to the DN. Therefore, the network becomes inoperative and hence the NL is determined and accumulated to arrive at 81, 292.4 + 77, 985.3 + 25, 595.2 $\approx$ 184, 873hrs after terminating the RL computation. Note that a single trial of the NL computation may be composed of a few iterations of the RL computations and it is not fixed to three iterations. It can vary depending on how much energy is utilized at the SN after each RL computation.

To elaborate further on how the sensor batteries are depleted after each iteration using the best route shown in Table 8, in Table 9 we provide the battery states for all sensors lying in the best route. We consider three states for the battery of sensor nodes lying on the best route. The "After" and "Before" states represent the level of all the sensor batteries in the network, except for the DN.

TABLE 8. One trial of NL computation is composed of three dependent steps of RL computation, while illustrating the level of SN battery after each iteration.

Iters	The best RL routes	RSS-LTED [J]	RL [hrs]	The best route	RBAT at SN [J]
1st	$[0 - 1 - 2 - 5]$	6163.22	81, 292.4	$[0 - 1 - 2 - 3 - 5]$	4887.3
	$[0 - 1 - 2 - 3 - 5]$	5733.57			
	$[0 - 4 - 1 - 2 - 5]$	9131.37			
	$[0 - 4 - 1 - 2 - 3 - 5]$	8444.52			
2nd	$[0 - 4 - 3 - 5]$	7310.61	77, 985.3	$[0 - 4 - 3 - 5]$	3155.44
	$[0 - 4 - 3 - 2 - 5]$	8164.02			
3rd	$[0 - 2 - 5]$	3490.03	25, 595.2	$[0 - 2 - 3 - 5]$	0
	$[0 - 2 - 3 - 5]$	3350.06			

TABLE 9. The battery state of all the sensor nodes after each iteration of RL computation in the WSN of Fig. 11.

Iters	The best route	State	Sensor nodes except DN $[0 - 1 - 2 - 3 - 4]$
1st	$[0 - 1 - 2 - 3 - 5]$	Before	$[5000 - 5000 - 5000 - 5000 - 5000]$
		Used	$[112.699 - 5000 - 14.821 - 606.048]$
		After	$[4887.3 - 0 - 4985.18 - 4393.95 - 5000]$
2nd	$[0 - 4 - 3 - 5]$	Before	$[4887.3 - 0 - 4985.18 - 4393.95 - 5000]$
		Used	$[1731.86 - 5000 - 578.755]$
		After	$[3155.44 - 0 - 4985.18 - 3815.2 - 0]$
3rd	$[0 - 2 - 3 - 5]$	Before	$[3155.44 - 0 - 4985.18 - 3815.2 - 0]$
		Used	$[3155.44 - 4.66644 - 189.95]$
		After	$[0 - 0 - 4980.51 - 3625.25 - 0]$

The "Used" state represents the amount of battery dissipation for the sensors lying on the best route utilized for the end-to-end transmission. Recall that node-0 is the SN and node-5 is the DN in Fig. 11. Since we assume that the ED at the DN is unimportant, because it is plugged into the mains power supply, the DN is removed from the battery charge update list. Therefore, only the first 5 nodes of the 6-node fully connected WSN of Fig. 11 is reserved for the battery charge update list. For example, each battery of the sensor nodes, in the order of $[0 - 1 - 2 - 3 - 4]$ is initialized with $[5000 - 5000 - 5000 - 5000 - 5000]$ Joules battery capacity, respectively and these nodes are always reserved in order and are updated, when a node is on the route utilized for the end-to-end transmission. Explicitly, depending on which route is used for an end-to-end transmission after each iteration of the RL computation, the corresponding battery of the sensor node is depleted in the WSN. For example, assuming that the sensors $[0 - 1 - 2 - 3 - 5]$ are utilized for the end-to-end transmission, only the actively utilized sensor battery charges are reduced by the amount of $[112.699 - 5000 - 14.821 - 606.048]$, respectively, as illustrated in Table 9. The battery of node-4 is never utilized in the first iteration, therefore in the state "After" of the first iteration it remains 5000J, while the residual battery charge of the other nodes becomes $[4887.3 - 0 - 4985.18 - 4393.95 - 5000]$.

Furthermore, for the sake of clarity we provide Fig. 12a, 12b, 12c, and 12d for illustrating which particular routes are utilized for end-to-end transmission, and hence which sensor batteries are updated after each iteration of the RL computation. Note that the hollow batteries represent the fully-depleted batteries after each iteration. Surprisingly, node-2 and node-3 were capable of preserving their battery levels as close as possible to their initial battery levels. This is due to the smaller distance between the transmitting node-2 and its receiver for the routes selected as the best RL-aware ones in each iteration. A similar trend is observed for node-3. For example, for the first iteration the distance between node-2 and node-3, as well as node-3 and node-5 is lower than those of others on the same route. Similar trends can be observed during the second and third iterations. Additionally, in the first iteration node-1, in the second iteration node-4 and in the third iteration SN (node-0) communicates over longer distances with their receivers compared to that of node-2 and node-3, respectively. Therefore, those sensor nodes depleted their batteries earlier than the other nodes lying on their respective routes, which are illustrated by the hollow batteries in Fig. 12b, 12c, and 12d, respectively.

5) SINGLE OBJECTIVE GENETIC ALGORITHM

The above run-time simulation analysis of ESA is based on $V = 6$ nodes, but it can be readily generalized for any arbitrary number of nodes. However, the computation of the NL strictly depends on the specific route's complexity in the WSN considered. For example, the $V = 6$ scenario of Fig. 11 examines 65 distinct non-looping alternative routes, whilst according to Table 3 $V = 10$ introduces 109,601 distinct routes for the NL computation using ESA. Therefore, the exponential increase in the number of distinct routes from 65 to 109,601 may impose an excessive complexity, especially when each NL computation requires more than a few RL computation iterations, which invokes a full search of the fully connected WSN during each iteration. This large number of distinct routes may correspond to a larger partially connected distributed network with many more sensor nodes. Therefore, our fully connected WSN approach can also be applied to any other realistic network without being limited to fully connected networks.

In order to circumvent the computational complexity of ESA encountered in realistic WSNs composed of a vast number of distinct routes we invoke a single-objective genetic algorithm (SOGA), which relies on genetic operations inspired by evolutionary biology, such as inheritance, selection, crossover, mutation and recombination. Before moving on to the intricate details of the SOGA considered, let us familiarize ourselves with the terms of evolutionary biology and its exploitation in our context. For example, a chromosome of the SOGA is composed of sequences of
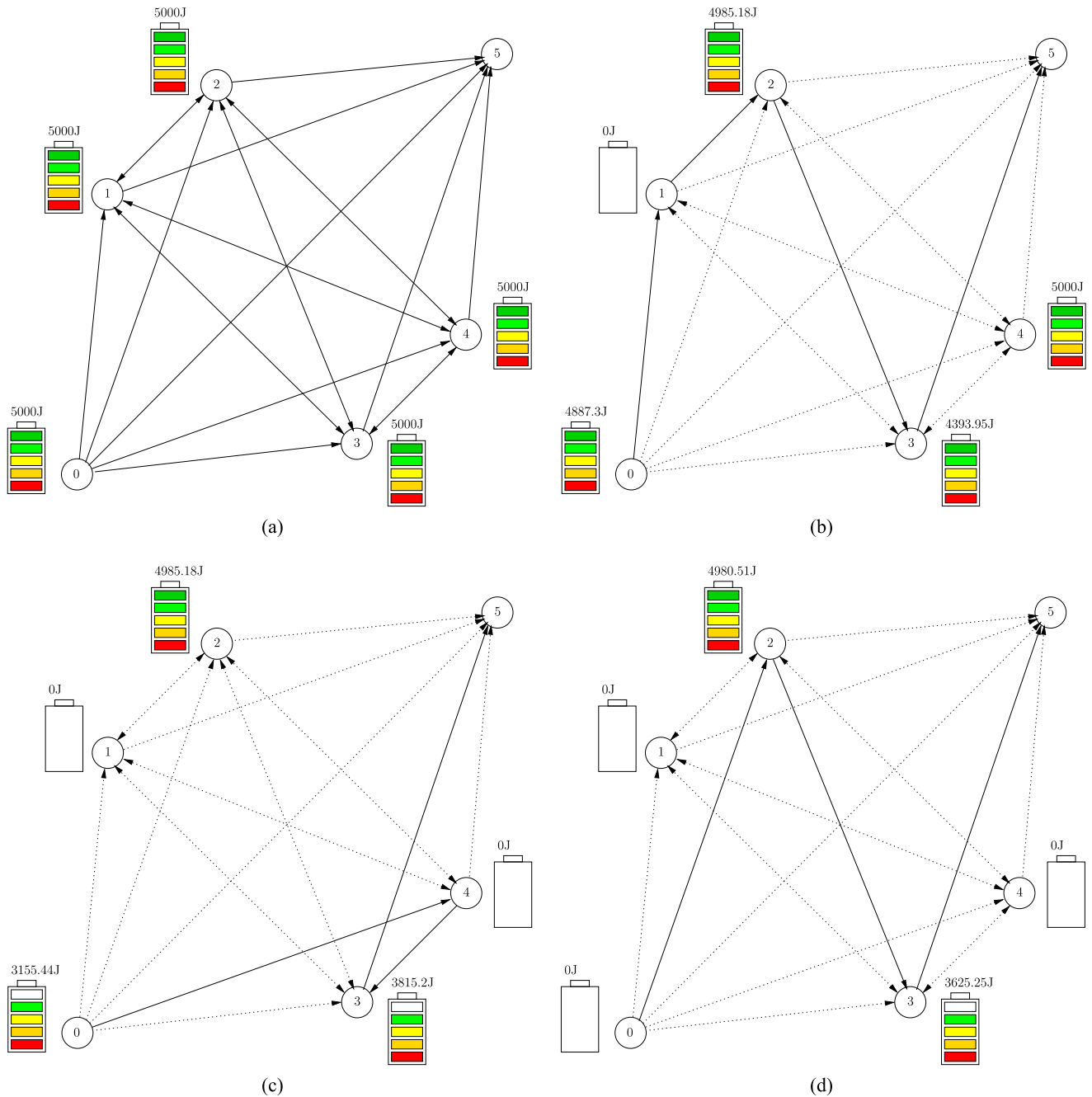
FIGURE 12. Illustration of the changes in the level of the battery-energy. (a) Initial battery level of all sensors in the WSN. (b) The battery levels after the first iteration of RL computation. (c) The battery levels after the second iteration of RL computation. (d) The battery levels after the third iteration of RL computation.

integers, which represent a specific route consisting of a unique sensor node index. Hence we refer to a sensor node as a gene, each of which belongs to the chromosome. We also refer to a chromosome as an individual of the SOGA having a specific route's path (chromosome) information. Moreover, a fitness function evaluates the quality of a chromosome in terms of achieving the desired objective. In our scenarios, we evaluate the route information of each individual using a fitness function or objective function to acquire the RL fitness value. Therefore, we can say that the fitness function

quantifies the quality of a chromosome (individual), where the fitness function is expected to have a higher fitness value in maximization problems for a better solution, i.e. route.

A general overview of how our SOGA operates is outlined in Fig. 13. The process commences with the initialization of a population, which is constituted by the individuals that are evaluated in terms of their specific fitness functions in order to identify the quality of the corresponding solutions. Note that we deploy a regular genetic algorithm, including some modifications of its operators. In a GA, a termination
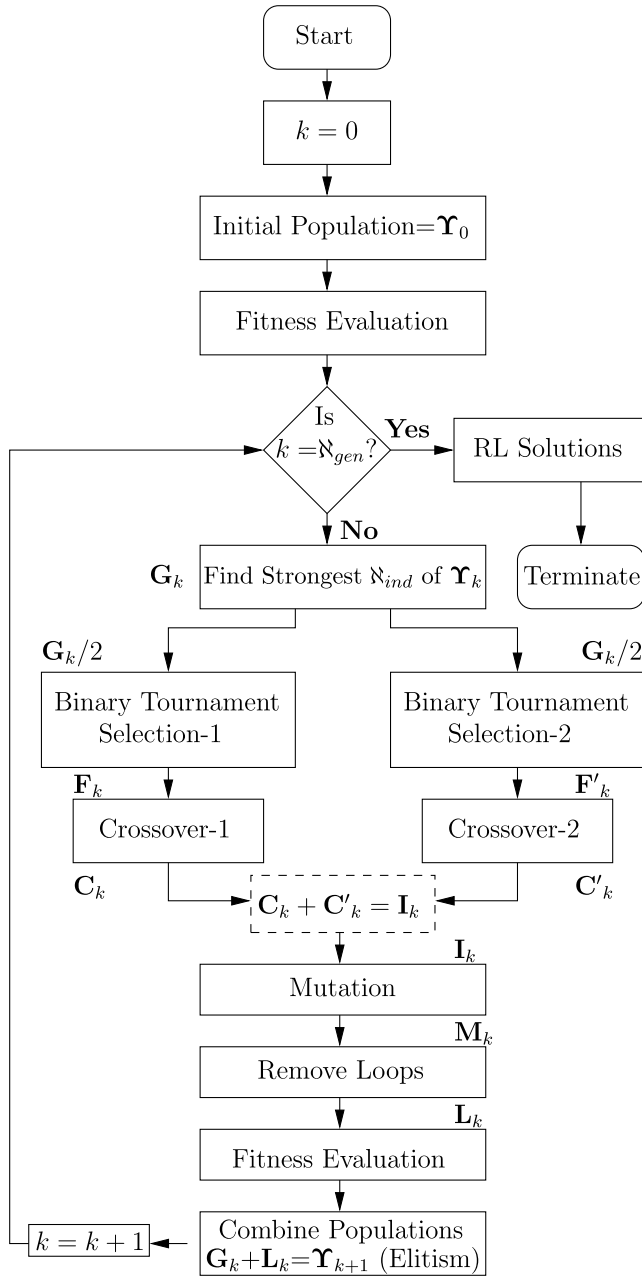
FIGURE 13. A flowchart presenting the general overview of the SOGA adopted for our NL maximization technique, which the flow of the genetic operations can also be followed for more details in Fig. 17.

their fitness characteristics to the next generations, as seen in Fig. 13. Consequently, we obtain the population $\mathbf{G}_k$ containing $\aleph_{gen}$ high-quality individuals, as illustrated in Fig. 13.

Following the inclusion of these high-quality individuals in the current population, we invoke the binary tournament selection (BTS) of Fig. 13, where the individuals of the current population are divided into two sets $\mathbf{G}_k/2$. Then, a specific individual is randomly selected from each of the two sets for a competition in terms of their fitness values. Finally, the particular individual having a better fitness value is selected as a parent individual for creating the next generation, which forms the populations $\mathbf{F}_k$ and $\mathbf{F}'_k$. Then, as seen in Fig. 13, the crossover operation is applied to each of these populations $\mathbf{F}_k$ and $\mathbf{F}'_k$ containing the parent individuals, respectively, for examining the current solutions in order to find more fit individuals, which may also introduce a certain grade of solution diversity for the current population. We use the single-point cross-over method, where a common gene (sensor node) is used for dividing the chromosomes into two parts for merging a certain fraction of the individual constituted by a route with the other half of the other individual and vice versa. These newly created individuals are termed as child individuals, which are expected to inherit the beneficial characteristics of the parent individuals. We note that as illustrated in Fig. 13, the BTS and crossover operations are applied twice for increasing the solution diversity as well as for acquiring a sufficient number of individuals. Then, the populations $\mathbf{C}_k$ and $\mathbf{C}'_k$, which are subjected to both the BTS and crossover operations, are combined in order to create the population $\mathbf{C}_k + \mathbf{C}'_k = \mathbf{I}_k$, which is then subjected to mutation, as seen in Fig. 13.

Finally, as seen in Fig. 13, a mutation operation is applied to the child individuals constituting the population $\mathbf{I}_k$, where each one of the genes of each child individual is mutated with a certain mutation probability, so that entirely new individuals constituting the population $\mathbf{M}_k$ can be introduced into the next generation. When the mutation operation is applied to a particular gene, we opt for one of three different mutation operations in our scenarios with equal probability, namely for node replacement, for node removal and for node insertion. Their specific details will be provided along with our more elaborate explanations of SOGA later in this section. Basically, the mutation operation further increases the diversity of the population by examining the fitness of new candidate solutions. Therefore, we may conclude that a population is created in the first generation (iteration) consisting of several individuals (candidate solutions) and throughout the successive generations by using the genetic operations described above. As a benefit, the individuals are expected to gradually create better solutions [51]–[53]. After the mutation operation, any potential node repetitions are removed from the routes, which leads to the population $\mathbf{L}_k$, as illustrated in Fig. 13. Then, the fitness of the individuals in population $\mathbf{L}_k$ is evaluated before proceeding to the forthcoming generation. Ultimately, as seen in Fig. 13, the newly created population $\mathbf{L}_k$ and the current population $\mathbf{G}_k$ are combined, since we

rule has to be set, so that it can terminate when a certain condition is satisfied, i.e. a sufficiently high quality solution has been found or the affordable number of generations has been exhausted. Specifically, in the SOGA we can adjust the number of generations $\aleph_{gen}$, as illustrated in Fig. 13, which allows us to strike a performance versus complexity trade-off. Additionally, since there are numerous individuals in a population, the specific selection amongst the candidate solutions (individuals) plays a significant role in terms of converging to an improved solution. Basically, the selection operator is invoked for improving the quality of the population by giving the high-quality individuals a higher chance of passing on

do not want to lose any of the current high-quality solutions. The specific process of combining the new and current populations as well as the technique of selecting the high-quality individuals from this combined population is referred to as elitism, which will be discussed later. Having summarized the general structure of a genetic algorithm and the SOGA considered, the diverse terminologies concerning the above genetic operations, including the individuals, populations, fitness values, binary tournament selection, crossover and mutation operations will be exemplified later in this section.

We simplified the multi-objective genetic algorithm described in [51] so that it can be utilized for single-objective optimization. We further modified the genetic operations in a manner similar to our work in [16]. One of the main differences between the SOGA and ESA is that SOGA intelligently searches through the solution space relying on the above-mentioned genetic operators, while ESA performs a brute-force full search by means of looking for all possible permutations in the solution space. As illustrated in Fig. 14, SOGA is capable of arriving at the best solution (marked by the largest dot filled with black color) after 5 generations, whereas ESA has to search though the entire solution space constituted by each dot for finding the best solution. However, the reduced-complexity SOGA may produce suboptimal results for large networks. Nonetheless, it may be configured to strike the required performance versus complexity trade-offs approaching the optimal NL. Let us now discuss the SOGA as described in Algorithm 2, where we mostly focus our attention on the genetic operators of the algorithm.
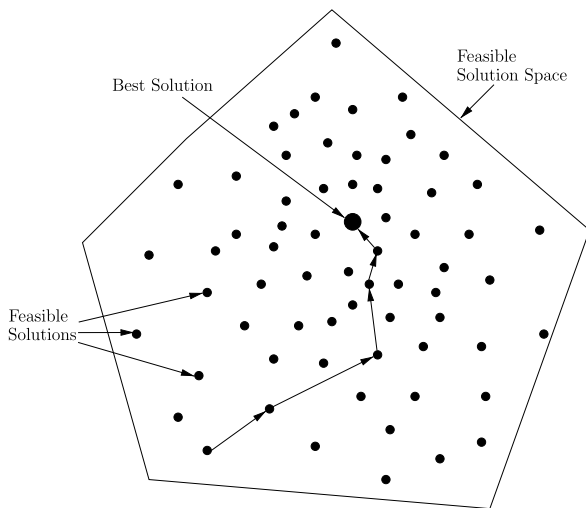

FIGURE 14. Solution search strategy of ESA and SOGA within the feasible solution space.

At the "input" section of Algorithm 2, we define the simulation parameters as well as the genetic operation constants, such as $\aleph_{ind}$, $\aleph_{gen}$, Pr_c, Pr_m denoting the number of individuals, number of generations, the crossover probability and the mutation probability, respectively. In each generation of a population, $\aleph_{ind}$ individuals are created, each of which

TABLE 10. Random route initialization of the 48 individuals in the first iteration of the first trial of the SOGA.

Individual index	Route information
0	$[0 - 4 - 1 - 2 - 5]$
1	$[0 - 4 - 1 - 3 - 2 - 5]$
2	$[0 - 4 - 1 - 3 - 5]$
$\vdots$	$\vdots$
35	$[0 - 1 - 3 - 2 - 4 - 5]$
$\vdots$	$\vdots$
46	$[0 - 1 - 2 - 4 - 3 - 5]$
47	$[0 - 3 - 1 - 2 - 4 - 5]$

represents a candidate solution, which is randomly initialized with feasible values during the initial population. After each iteration of $\aleph_{gen}$, these initialized individuals are expected to converge to superior fitness values by applying the genetic operators of inheritance, selection, crossover, mutation and recombination, which also assist us in increasing the diversity of the solutions, so that the algorithm would not miss the improved solutions. Firstly, we create a fully connected, randomly and uniformly distributed WSN and obtain the distance matrix of it with the aid of coordinates of the sensors, as indicated on line 3 and 4 of Algorithm 2. Then, an initial population associated with $\aleph_{ind} = 48$ individuals is created and each individual is associated with a route randomly selected from the fully connected WSN, as shown on line 7–9 of Algorithm 2 and in Table 10. Here, we only gather the route information of the individuals, but the RL objective function or synonymously the fitness function, is not evaluated. Hence we have no knowledge of the fitness values for the corresponding individuals. Therefore, on line 10 of Algorithm 2 these routes are passed to the dual-simplex optimization function in conjunction with their respective distance matrices for the RL evaluation, where each RL evaluation is characterized in terms of its fitness value. Hence, in our case each function call to the dual-simplex optimization function produces a fitness array consisting of the RL, the energy used per node and the transmit power per link utilized. The $\aleph_{ind}$ number of individuals (candidate solutions) are selected from population Υ_k as the set of strongest individuals denoted by $\mathbf{G}_k$. As the iterations (generations) progress, Υ' is returned in conjunction with $(2 \times \aleph_{ind})$ individuals at the end of each generation. Therefore, the selection process[8] of the strongest individuals guarantees having $\aleph_{ind}$ individuals

---

[8]This selection process introduces elitism to SOGA, where the better individuals from previous generations are carried over the next generations, unchanged. Therefore, the solution quality will never decrease from one generation to the next, since the best solution from previous generations is kept throughout the next generations. This selection strategy is known as elitist selection, which is not to be confused with the BTS.

Algorithm 2 SOGA for Maximizing the NL Based on the Battery Level of the SN

Input: γ (target SINR)

      τ (number of trials)

      $\mathcal{E}_{init}$ (initial battery of each sensor in the WSN)

      V (number of nodes)

      $(x_{max} \times y_{max})\text{m}^2$ (size of the sensor field starting from $(0, 0)$ to (x_{max}, y_{max}))

      κ (total number of RSS, while i indicates each of the RSS)

      T_{net} (network lifetime)

      $\aleph_{gen}$ (number of generations)

      $\aleph_{ind}$ (number of individuals)

      Pr_c (probability of crossover)

      Pr_m (probability of mutation)

1:   **for** i **from** 0 **until** κ **do**
2:     **for** j **from** 1 **until** τ **do**
3:       Create a fully connected, randomly and uniformly distributed network for V
4:       $d_{all} \leftarrow$ Get distance matrix using coordinates of sensors lying on $(x_{max} \times y_{max})\text{m}^2$
5:       $T_{net} = 0 \leftarrow$ Set initial value of NL to zero per created network
6:       **function** run($\mathcal{E}_{init}$, T_{net}, γ) $\rightarrow$ Start SOGA
7:       create(Υ_0) $\leftarrow$ Create an initial population
8:       $\Upsilon_0 \rightarrow \mathbf{R} \leftarrow$ Create $\aleph_{ind}$ random routes for setting up the population
9:       $\Upsilon_0 \rightarrow T_{\mathbf{R}} = 0 \leftarrow$ Initialize the RL of each individuals in the population
10:      dual-simplex($\Upsilon_0 \rightarrow \mathbf{R}$, d_{all}, $\mathcal{E}_{init}$, γ) $\rightarrow$ Evaluate RL of $\Upsilon_0 \rightarrow \mathbf{R}$
11:      **for** k **from** 0 **until** $\aleph_{gen}$ **do**
12:        $\mathbf{G}_k \leftarrow$ get-strongest-$\aleph_{ind}(\Upsilon_k)$
13:        $\mathbf{F}_k \leftarrow$ get-$\aleph_{ind}/2$-parents($\mathbf{G}_k$), binary tournament selection
14:        $\mathbf{C}_k \leftarrow$ get-$\aleph_{ind}/2$-crossover-$\aleph_{ind}/4$-by-$\aleph_{ind}/4(\mathbf{F}_k)$ using Pr_c
15:        $\mathbf{F}'_k \leftarrow$ get-$\aleph_{ind}/2$-parents($\mathbf{G}_k$), binary tournament selection
16:        $\mathbf{C}'_k \leftarrow$ get-$\aleph_{ind}/2$-crossover-$\aleph_{ind}/4$-by-$\aleph_{ind}/4(\mathbf{F}'_k)$ using Pr_c
17:        $\mathbf{I}_k \leftarrow$ complete-individuals-to-$\aleph_{ind}(\mathbf{C}_k + \mathbf{C}'_k)$
18:        $\mathbf{M}_k \leftarrow$ mutate-individuals-get-$\aleph_{ind}(\mathbf{I}_k)$ using Pr_m
19:        $\mathbf{L}_k \leftarrow$ remove-loops-of-$\aleph_{ind}(\mathbf{M}_k)$
20:        dual-simplex($\mathbf{L}_k \rightarrow \mathbf{R}$, d_{all}, $\mathcal{E}_{init}$, γ)
21:        $\Upsilon_{k+1} \leftarrow$ combine-populations-get-$2 \times \aleph_{ind}(\mathbf{L}_k, \mathbf{G}_k)$
22:      **end for**
23:      $\mathbf{T}_{\mathbf{R}} \leftarrow$ Return the route lifetime of $\Upsilon'_{\aleph_{gen}} \rightarrow \mathbf{R}$
24:      $\mathbf{E}_{\mathbf{R}} \leftarrow$ Return the energy usage per node of $\Upsilon'_{\aleph_{gen}} \rightarrow \mathbf{R}$
25:      $\mathbf{P}_{\mathbf{R}} \leftarrow$ Return the transmit power per link of $\Upsilon'_{\aleph_{gen}} \rightarrow \mathbf{R}$
26:      $T_R \leftarrow$ Obtain maximum $\mathbf{T}_{\mathbf{R}}$
27:      $\mathbf{R}_{best} \leftarrow$ Reserve the best RL aware routes with T_R
28:      **do while** $\mathcal{E}_{SN} > 0 \leftarrow$ NL strictly depends on the SN battery level
29:        $T_{net} = T_{net} + T_R \leftarrow$ Accumulate each RL value for building the NL
30:        $R_{best} \leftarrow$ Select the best route using RSS$_i$ from $\mathbf{R}_{best}$ for end-to-end transmission
31:        $\mathbf{R}_{final} \leftarrow$ Copy R_{best} to a final array for each iteration of RL.
32:        Update the batteries of all sensors with $E_{R_{best}}$ to obtain $\mathcal{E}_{residual}$
33:        **return** run($\mathcal{E}_{residual}$, T_{net}, γ)
34:      **end do**
35:      E2EB computation as between line 26 and 31 of the Algorithm 1
36:     **end for**
37:   **end for**
38:   **return** averaged T_{net} and worst case E2EB over τ trials for each RSS

---

for the current population associated with the strongest attributes. The population $\mathbf{G}_k$ having $\aleph_{ind}$ individuals is randomly divided into two halves each having $\aleph_{ind}/2$ individuals of the population $\mathbf{F}_k$ in order to find the parents based on the BTS, as illustrated in Table 11 for crossover operation on line 13. We note that in Table 11 each index value

TABLE 11. The indices of the selected parents after BTS operation of *Pair₁* and *Pair₂* in the first iteration of the first trial of the SOGA.

Pairs	The index order of the individuals for BTS
$Pair_1$	{24, 12, 23, 29, 18, 8, 17, 6, 22, 1, 4, 20, 14, 11, 25, 0, 5, 16, 44, 9, 41, 2, 35, 34}
$Pair_2$	{30, 46, 28, 3, 45, 40, 37, 33, 7, 42, 21, 38, 47, 27, 43, 31, 36, 10, 26, 19, 32, 15, 13, 39}
Parents	{24, 12, 23, 3, 18, 8, 17, 6, 7, 1, 4, 20, 14, 11, 25, 0, 5, 16, 26, 9, 32, 2, 13, 34}

represents an individual. Despite the fact that the index of 48 individuals is uniquely divided into two pairs of *Pair₁* and *Pair₂*, the route information these individuals refer to can be exactly the same. For example, in Fig. XI, the individuals 24 and 30 are supposed to be different individuals due to their unique index values. However, the route information of the individuals 24 and 30 can be exactly the same. Nonetheless, the genetic operations can be extended to a strategy for creating arbitrary non-replicative individuals in the genetic algorithm considered, which provides us with a potentially faster convergence, since the algorithm is naturally forced to provide a higher grade of diversity of solutions at the initial stage. Note that BTS assists us in obtaining moderately stronger parent individuals associated with better fitness values for crossover operation. However, the BTS cannot guarantee that the selected individuals will always be stronger. More explicitly, in Table 11, *Pair₁* and *Pair₂* are compared in terms of their fitnesses and the better individuals are listed as "Parents". For example, individuals 24 and 30 are compared in terms of their fitnesses and 24 is selected as a better individual, since its RL evaluation produced a better fitness value for its route information. However, the fitness value of eliminated individual 30 for its route could have been better than that of the next elected individual, namely 12 in the current population $\mathbf{F}_k$. Therefore, BTS can only advocate the selection of fairly stronger individuals, while maintaining a beneficial solution diversity, which prevents early convergence by exploring much of the search-space. On line 14 of Algorithm 2 ($\aleph_{ind}/2$) individuals of

the population $\mathbf{F}_k$ are consecutively divided into two halves, each of which now contains $\aleph_{ind}/4$ parent individuals. The pair sets of parent individuals, i.e. {(24, 12), (23, 3), (18, 8), ..., (13, 34)} of Table 11, are then mated with the aid of the crossover operation as exemplified in Fig. 15 using Pr_c in order to create two child individuals, which may inherit attributes of both fairly strong parents selected by the BTS. Explicitly, assume that two consecutive arbitrary parents {... (1, 35) ...} selected from Table 10 exist in the population $\mathbf{F}_k$ for the sake of illustrating the crossover operation in Fig. 15. At the instant of the crossover operation, we use a similar strategy to that of our work in [16], where a common sensor node is chosen for the crossover point in our scenarios considered. We assume that the parents $Parent_1$ and $Parent_2$ represent the individuals 1 and 35 of $\mathbf{F}_k$, respectively. In this particular scenario, as illustrated in Fig. 15 the common node is selected as 3 for both $Parent_1$ and $Parent_2$. Then, $Child_1$ is created by the concatenation of the specific parts of the individuals representing the nodes leading up to and including the common node 3 from $Parent_1$ with the nodes following 3 in $Parent_2$ and similarly for $Child_2$. Then, the newly created two sets of child individuals are merged to a total number of $\aleph_{ind}/4 + \aleph_{ind}/4 = \aleph_{ind}/2$ individuals. However, to obtain the original population size of $\aleph_{ind}$, lines 15 and 16 of Algorithm 2 are applied again as the operations on lines 13 and 14 of Algorithm 2. More explicitly, both BTS and the crossover operations are applied twice to the current population in order to obtain $\aleph_{ind}$ individuals of the population $\mathbf{I}_k$, as indicated on line 17 of Algorithm 2.
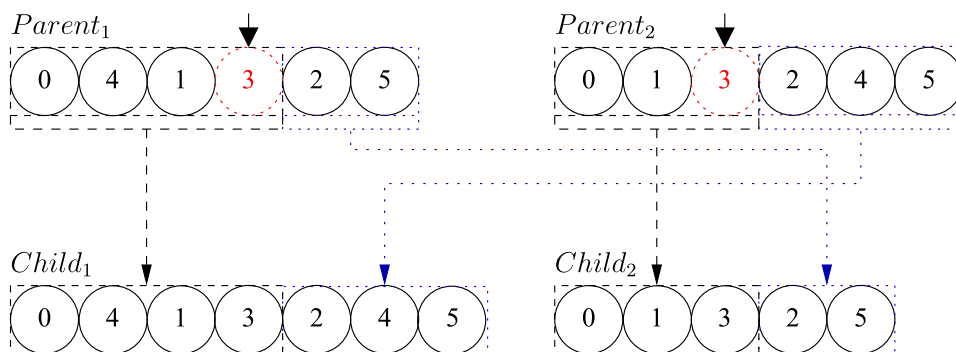
FIGURE 15. Crossover operation of parent individuals (1, 35), where *Parent₁* and *Parent₂* represent individual 1 and 35 of F_k, respectively.
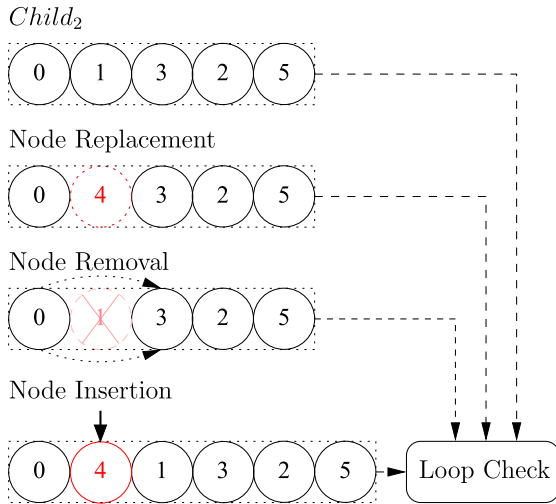
Child$_2$

FIGURE 16. Mutation operations of *Child$_2$*, which is created by the crossover operation of the parent individuals (1, 35) of F_k.

Further clarifications concerning the changes of the population size are provided in Fig. 17, while the genetic operators continue to iterate from the initial population Υ_0 to the final population Υ'_k throughout k generations. Moreover, in our scenarios a similar mutation method to that of our work in [16] is applied to each sensor node (gene) lying on a route of an individual (candidate solution, chromosome or route) with the probability of Pr_m. In the implementation of the mutation operator, three possible modifications are invoked with equal probability, such as the node replacement, node removal and node insertion. In case of node replacement, the current node is replaced with a randomly selected node, as shown in Fig. 16. In node removal, the current node is removed from its route and the previous node is linked with the latter node. In case of node insertion, a randomly selected new node is inserted before the current node. After mutation is applied to each individuals, any potential node repetitions imposed are removed from each route in the interest of improving the population-diversity.

IV. EXPERIMENTAL RESULTS

We consider a fully connected network associated with $V = \{4, 5, 6, 7, 8, 10, 15, 20\}$ nodes, where for example $V = 7$ is composed of 326 and $V = 10$ is composed of 109, 601 distinct non-looping routes, as indicated in Table 3. A fully connected network is considered, because it may have an excessive number of links upon increasing the number of sensor nodes, when we aim for investigating the complexity of the distinct routes for a given WSN. Therefore, our implementation of a fully connected network may be applied to any distributed network having more nodes, but with less number of communicating links. Specifically, we consider a sensor field of $40 \times 40\text{m}^2$ for a WSN having V sensor nodes. The SN and the DN are placed at the opposite corners of the sensor field, where the SN is placed at the coordinate of $(0, 0)$ and the DN is located at the coordinate of $(40, 40)$, which guarantees

having the longest distance between the SN and the DN at all time. This specific SN and DN placement is important, because a single-hop transmission from SN to DN is not a favorable option due to its highest transmit power required over the longest distance amongst all the other distinct routes. Therefore, the end-to-end transmission across the network is designed for the sake of NL maximization by the evaluation of the various routes across the WSN considered. We note that the experimental results of the NL are obtained for a continuous transmission scenario, termed as 'continuous-time NL'. For brevity, we simply use the term 'NL' for 'continuous-time NL'. On the other hand, in this paper the NL values are expected to be much higher than those of our previous papers [14] and [15] owing to the specific NL definition considered. Explicitly, in our previous papers [14] and [15] the NL was computed for a string topology, where the distances are fixed, hence a sensor does not have the option of transmitting over another lower-dissipation route. However, in our scenario the SN is capable of exploiting alternative routes with the aid of a greedy-ED approach, by selecting the maximum RL-aware route for the end-to-end transmission in a fully connected WSN, where the aim is to carry the information generated at the SN to the DN until the SN battery is fully depleted. More explicitly, the accumulation of the maximum RL computed over the alternative routes provides us with a substantially extended NL, since the NL computation is composed of the summation of the several RL values, until the SN battery is fully depleted. Moreover, the maximum affordable transmit power of each node is set to $(P_i)_{max} = 0.01\text{W}$, as in the IEEE Standard 802.15.4 [54]. We consider an AWGN channel, which is defined by a certain propagation path loss model having the path loss exponent of $m = 3$ and a fixed noise power of $N_0 = -60\text{dBm}$ at the receiver. Since the sensors communicate over the same shared channel, we utilize a TDMA based scheduling scheme we defined in Section II-A, namely the SPTS with $T = 3$, where each link relies on a TDMA frame consisting of $N = 3$ TSs. The target SINR thresholds per link are defined as $\gamma = \{0, 0.5, 1, \ldots, 9, 9.5, 10\}\text{dB}$ in order to investigate the NL performance of the WSN considered, where each link operates over different sets of target SINR values. Each sensor is equipped with an AAA long-life alkaline battery having the capacity of 5000J. For convenience, we summarize the system parameters used in our simulations in Table 12. In all scenarios of the SOGA, we set $\aleph_{ind} = 48$. These parameters are utilized in each iteration of the RL computation for each NL trial and the NL is averaged over $\tau = 5000$ trials. We use the number of CFEs to measure the complexity by accumulating each fitness evaluation call to the dual-simplex function, until a NL value is calculated by the ESA and SOGA described in Algorithm 1 and Algorithm 2, respectively. In some of our analysis, the target SINR value or RSS is not specified, because we only compare the complexity of the algorithms. Therefore, as an example we choose the results of $\gamma = 0\text{dB}$ and/or RSS-LTED, unless stated otherwise. For example, for any SINR value other than $\gamma = 0\text{dB}$,
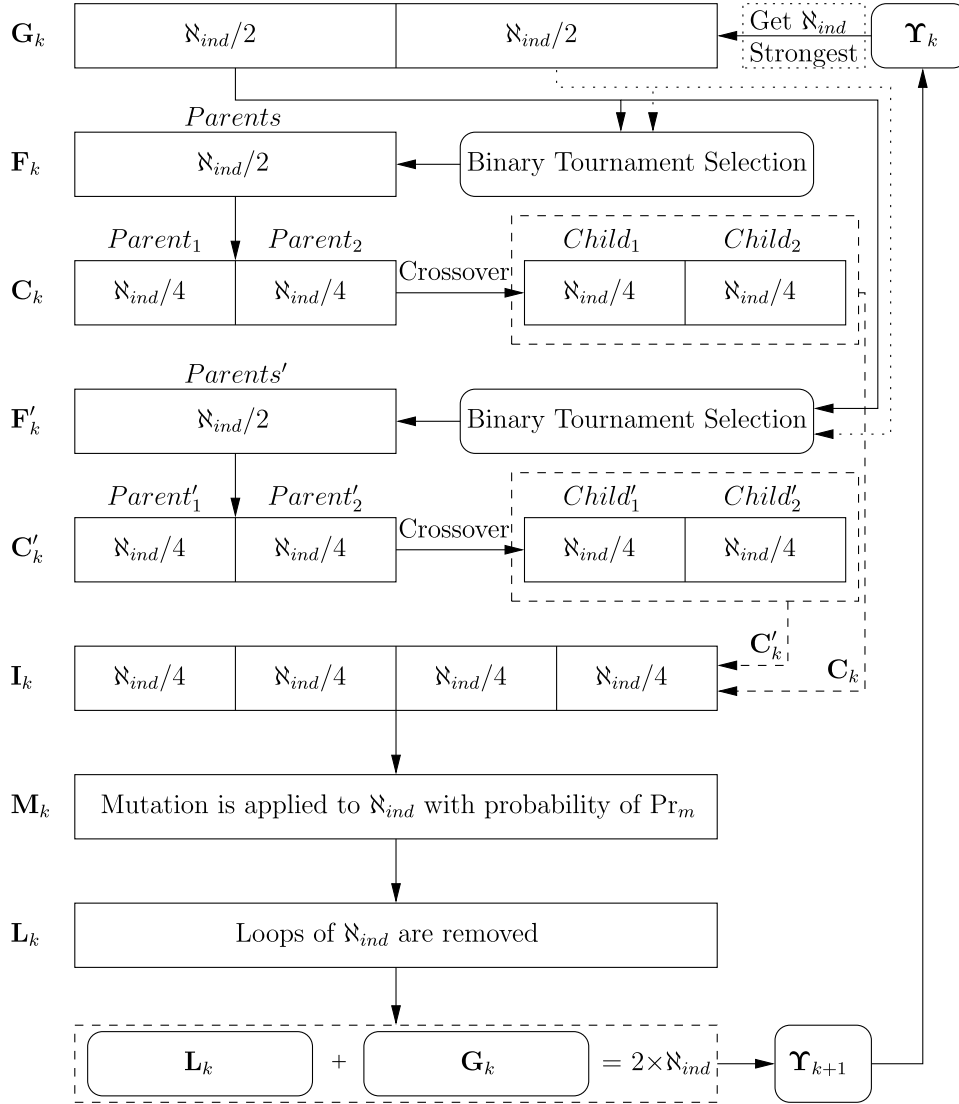
FIGURE 17. Illustration of the changes in the population size, while the genetic operations iterate.

we observe the same complexity for the same algorithm, hence the number of CFEs is independent of both the target SINR value and of the RSS.

A. DIFFERENCE WITH RESPECT TO THE OPTIMAL NL VERSUS COMPLEXITY

The optimality analysis of the SOGA is provided in Fig. 18 for the sake of NL maximization, while considering $\aleph_{gen} = \{3, 12\}$ generations for $V = \{4, 6\}$ sensor nodes, as well as $\aleph_{gen} = \{3, 15, 18\}$ generations for $V = 8$ sensor nodes, and $\aleph_{gen} = \{9, 21, 24\}$ generations for $V = 10$ sensor nodes. The target SINRs are set to $\gamma = \{0, 0.5, 1, \dots, 9, 9.5, 10\}$. Note that here we consider the NL achieved by the RSS-LTED, but the other RSSs also exhibit similar trends. It is observed that for a lower number of nodes the convergence to the optimal NL can be readily

obtained with the aid of a lower number of generations. For example, in Fig. 18 we can see for $V = 4$ that the NL results always match the optimal NL values after a few generations. Therefore, for $V = 4$ this emphasizes that there is no further improvement in the NL results upon increasing N_{gen}, which would introduce unnecessary additional complexity. However, upon increasing V, increasing the complexity becomes inevitable for the sake of attaining the optimal NL. For instance, for $V = 6$ there is a slight reduction in the performance of the SOGA for $\aleph_{gen} = 3$, when aiming for attaining the optimal NL obtained using the ESA. For a fixed number of generations, such as $\aleph_{gen} = 3$, the gap between the optimal and the suboptimal NL values further increases upon increasing V. This is because the number of distinct non-looping routes exponentially increases, as indicated in Table 3. Hence obtaining a near-optimal NL necessitates investing a higher computational complexity,

TABLE 12. System parameters utilized in our simulations.

Simulation parameter	Value
Channel model	AWGN
Path loss exponent, m	3
Target SINR per link $l_{i,j}$, γ [dB]	$\{0, 0.5, 1, ..., 9, 9.5, 10\}$
Noise power, N_0 [dBm]	-60
Battery capacity per sensor, $\mathcal{E}_i$ [Joule]	5000
Maximum transmit power of a node, $(P_i)_{max}$ [mW]	10 [54]
Number of TSs per frame, N	3
The field size of the WSN [m^2]	40×40
Number of nodes, V	$\{4, 5, 6, 7, 8, 10, 15, 20\}$
Number of trials per NL, τ	5000
Efficiency of the power amplifier, α	0.6 [55]
SPTS parameter, T	3
Number of total RSSs	4
Number of generations, $\aleph_{gen}$	$\{3, 6, 9, 12, 15, 18, 21, 24\}$
Number of individuals, $\aleph_{ind}$	48
Probability of crossover, Pr_c	0.9
Probability of mutation, Pr_m	0.5

where a higher $\aleph_{gen}$ is required. For example, for $V = 10$ the difference between the NL solutions for various $\aleph_{gen}$ values is significant, especially for $\aleph_{gen} = \{9, 21\}$. This is because the SOGA leads to a suboptimal NL at a reduced complexity, i.e. for $V = 10$ and $\aleph_{gen} = 9$, whereas the SOGA is capable of approaching the optimal NL value, which is only possible at the cost of a higher complexity, i.e. for $V = 10$ and $\aleph_{gen} = 21$. Therefore, the complexity versus the discrepancy with respect to the optimal NL plays a significant role in characterizing the system model considered, which will be discussed later in this section. Nonetheless, when the WSN operates at SINR = 2dB, a NL improvement of approximately 45,000hrs is achieved with the aid of an additional sensor node, for example when a 5th sensor is admitted to the 4-node fully connected WSN or a 6th sensor node is admitted to the 5-node fully connected WSN and so on. However, the NL improvement is reduced to about 5,500hrs, when the WSN operates at SINR = 10dB for the system

model considered. Another significant finding is that to obtain a near-optimal NL when V increases, we have to increase $\aleph_{gen}$, which in turn increases the computational complexity imposed. The ESA is considered as the best possible solution for the NL evaluation, which is an upper bound to the true NL attained by the SOGA. In Fig. 19, the SOGA is seen to be capable of achieving the optimal NL with the aid of $\aleph_{gen} = 3$ for $V = \{4, 5\}$. However, the $V = \{6, 7, 8, 10\}$ scenarios require a larger $\aleph_{gen}$ for approaching the optimal NL. For example, when considering $V = \{6, 7\}$, the SOGA is only capable of achieving suboptimal NL solutions for $\aleph_{gen} = 3$, but when we have $\aleph_{gen} = 6$, the NL becomes near-optimal for $V = 6$ and for $\aleph_{gen} = 9$ the NL gap with respect to the ESA benchmark becomes extremely small for $V = 7$. Therefore, in the following investigations, we consider that for $V = \{4, 5\}$ using $\aleph_{gen} = 3$, for $V = 6$ using $\aleph_{gen} = 6$, for $V = 7$ using $\aleph_{gen} = 9$, for $V = 8$ using $\aleph_{gen} = 15$ and for $V = 10$ using $\aleph_{gen} = 21$ constitute an attractive compromise,
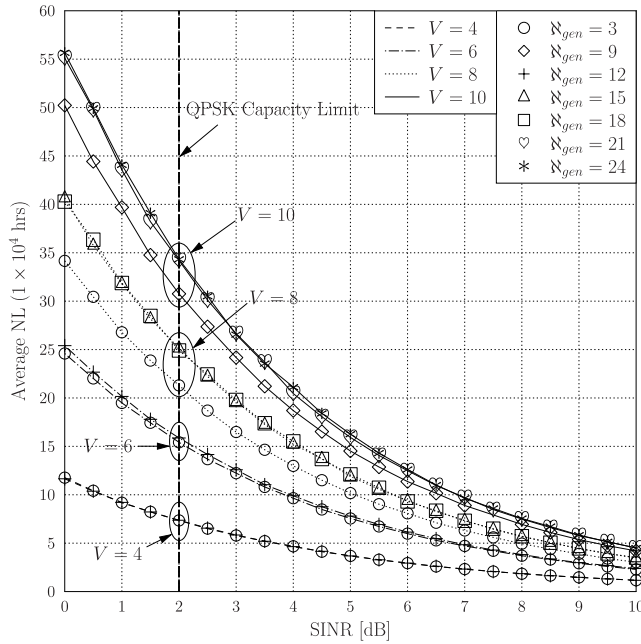
FIGURE 18. The NL of the SOGA invoked for the sake of NL maximization considering various parameter values of $\aleph_{gen}$, γ and V.
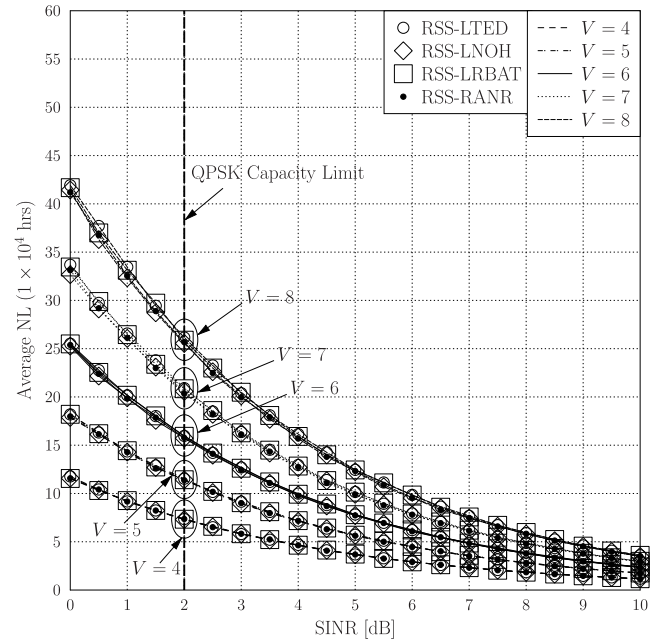

FIGURE 20. NL of different RSSs in the ESA for various V and γ values.
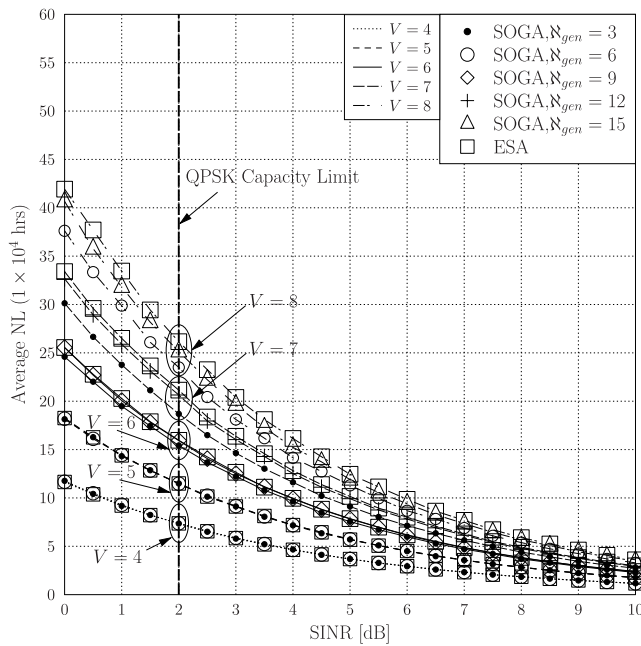

FIGURE 19. ESA as an upper bound for the true NL compared to the NL of SOGA for various $\aleph_{gen}$ and V values.

when aiming for obtaining a near-optimal NL value at the cost of a reasonable complexity.

B. NL PERFORMANCE OF VARIOUS RSSs USING THE ESA AND SOGA

Fig. 20 characterizes the NL of the RSSs of ESA considering various V and γ values. As mentioned in Section III-B2, RSSs are introduced due to multiple routes having the same

maximum RL. Therefore, the selection of the route in this stage plays a significant role in determining the NL, because the best route selected will be utilized for the end-to-end transmission and therefore the battery of the sensors utilized is correspondingly drained and updated for the next iteration. For a lower V, such as for example $V = 4$, the differences between the RSSs are negligible. However, for $V = 7$ we only have small differences in the NL of the RSSs considered. This is because there are many distinct non-looping routes for the fully connected network composed of a higher number of nodes V, and hence the probability of having a variety of best routes in each iteration of RL computations is high in terms of the LTED, LNOH, LRBAT and RANR. For example, for $V = 7$ at SINR of 2dB the optimal NL for RSS-LTED is the highest, followed by RSS-LRBAT, then RSS-RANR and finally, RSS-LNOH. We expect that the NL of RSS-LRBAT and RSS-LTED becomes moderately better than the other two RSSs owing to their energy awareness. More explicitly, RSS-LTED is based on the least total ED of the route, while RSS-LRBAT relies on the SN's battery level. Therefore, we observe that in our scenarios RSS-LRBAT and RSS-LTED typically outperform RSS-RANR and RSS-LNOH in terms of their NL, which can be readily seen in Fig. 20 and Fig. 21. Specifically, when a higher number of nodes V is considered, the difference in NL can be readily observed.

Rather than providing the NL results associated with all $\aleph_{gen}$ values for different WSNs composed of V sensor nodes, as previously mentioned, we only consider the near-optimal NL characteristics of SOGA associated with their near-optimal $\aleph_{gen}$ choices, as indicated in Fig. 21. It becomes clear in Fig. 21 that for the near-optimal $\aleph_{gen}$ choices and for their respective WSNs composed of V sensor nodes, the maximum
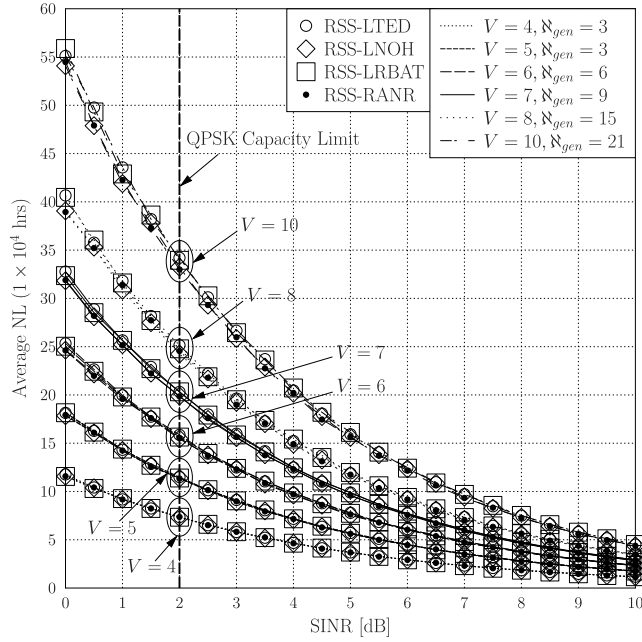
FIGURE 21. NL of different RSSs in the SOGA for various *V* and *γ* values.

FIGURE 22. The NL versus complexity of SOGA for a WSN composed of *V* sensor nodes.

NL attained by SOGA approaches that of its benchmark NL values, as illustrated in Fig. 19. We observe that similar to Fig. 20 a near-optimal NL is obtained for the corresponding RSSs by SOGA in Fig. 21.

C. THE NL VERSUS COMPLEXITY TRADE-OFF

The NL versus routing complexity trade-off plays a significant role in characterizing the system model considered. It will be demonstrated that SOGA is capable of achieving a near-optimal NL in conjunction with $\aleph_{gen} = 15$ at a much lower complexity for a WSN having $V = 8$ nodes, as illustrated in Fig. 19. Furthermore, SOGA is capable of finding route resulting in a near-optimal NL value for a WSN consisting of $V = 10$ nodes. Here, due to the high computational complexity of ESA, the optimal NL achieved by the ESA is not provided for WSNs having $V > 8$ nodes, which consist of more than 1,957 distinct non-looping routes. One may think that increasing V from 8 to 10 imposes an insignificant change in complexity. However, in our scenarios we consider the distinct non-looping routes of a fully connected WSN, which leads to an exponential increase in the computational complexity. Correspondingly, increasing V from 8 to 10 increases the number of distinct non-looping routes from 1,957 to 109,601, which is a substantial escalation of the computational complexity, and whilst the SOGA can cope with it, the ESA cannot. The computational complexity of both the ESA and SOGA is proportional to the average number of CFEs required for the computation of a specific NL value. Therefore, the attainable NL associated with their required number of CFEs is illustrated in Fig. 22. More explicitly, the convergence of the computed NL to the optimal achieved at the cost of the complexity required by the
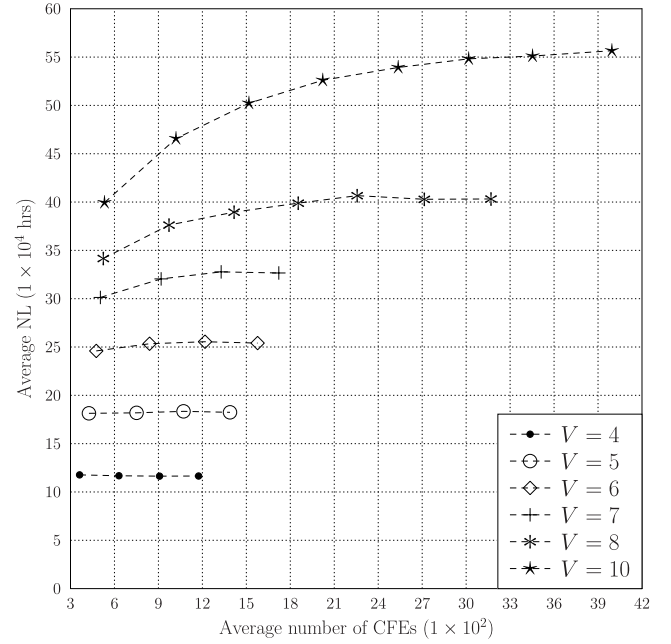
SOGA can be readily seen from Fig 22, which also explains the optimal choices of $\aleph_{gen}$ provided in Fig. 21. Note that in Fig 22, the vertical points of the different markers represent the computed NL value for each $\aleph_{gen}$, which is incremented by 3 from left to right for each fully connected WSN composed of V nodes. In terms of the attainable NL, increasing $\aleph_{gen}$ from 3 to 12 with intervals of 3 for $V = \{4, 5\}$ does not improve the NL, but imposes unnecessary complexity, while the NL of the $V = \{6, 7\}$ scenarios barely improves upon increasing $\aleph_{gen}$ from 3 to 12. However, the $V = 10$ scenario results in a significant NL improvement for each increase of $\aleph_{gen}$ from $\aleph_{gen} = 3$ to $\aleph_{gen} = 21$, when it is seen to converge to its optimal NL value at $\aleph_{gen} = 21$.

The number of CFEs required for the NL computation by the ESA and SOGA for V number of nodes is illustrated in Fig. 23, where the NL of SOGA is computed for each of the $\aleph_{gen}$ values considered. For each fully connected WSN composed of V nodes, the number of CFEs required for achieving the optimal NL can be compared to that of ESA as an upper bound to the true NL. We also illustrated in Fig. 23 number of the CFEs required for attaining the near-optimal NL for each WSN composed of V sensor nodes. Moreover, Fig. 23 illustrates that the ESA outperforms the SOGA for $V \leq 7$, when aiming for near-optimal NL values. This is a benefit of the higher number of individuals $\aleph_{ind} = 48$ evaluated in each iteration of $\aleph_{gen}$. Therefore, in each iteration of the RL computation, the routes represented by the $\aleph_{ind} = 48$ individuals are evaluated and this requires at least 48 CFEs. Note that a single NL computation may require a few RL computation iterations, hence it may lead to a higher number of CFEs. However, in the least complex
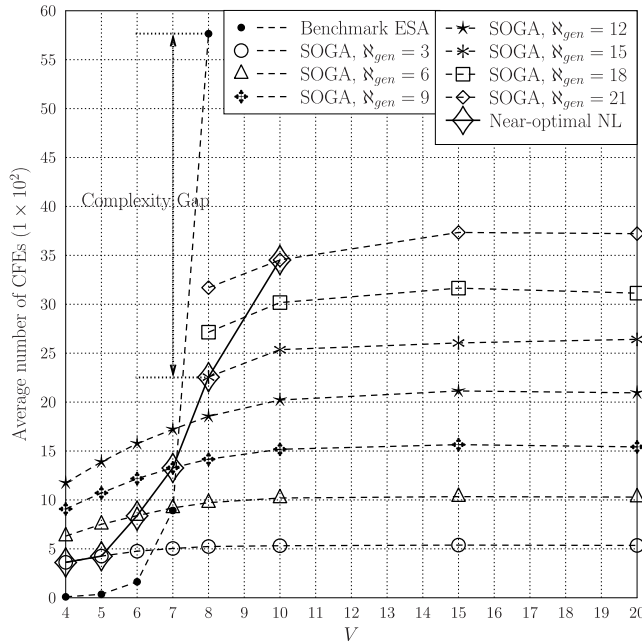
FIGURE 23. Complexity analysis of the ESA and the SOGA for *V* nodes, given $\aleph_{gen}$ for the SOGA.

scenario, where a single iteration of RL computation fully drains the SN battery and produces the NL value, 48 CFEs will be required, which already necessitates a larger number of CFEs than in the scenarios of $V \leq 7$ for the ESA. In Fig. 23, we can observe that $V = 7$ is the point, where the computational complexity of the ESA is similar to that of the SOGA and increases exponentially, when $V > 7$. Therefore, we may conclude that the SOGA imposes a lower complexity than the ESA for WSN having $V > 7$ nodes. For example, observe in Fig. 23 that the SOGA is capable of finding a near-optimal NL for $V = 8$ at a 2.56 times lower complexity than the ESA. Another important conclusion is that the complexity imposed by finding the near-optimal NL values in SOGA increases near-linearly upon increasing V, whereas the complexity of spotting the optimal NL values in the ESA increases exponentially. For example, the complexity of the optimal NL, when moving from $V = 6$ to $V = 7$ in the SOGA is provided in Fig. 23, where the number of CFEs is increased 1.58 times. Similarly, the complexity of the optimal NL upon extending the network from $V = 7$ to $V = 8$ in the SOGA is increased 1.70 times. We expect this gap to be much larger for the ESA due to its exponentially increasing complexity. For example, upon extending the network from $V = 6$ to $V = 7$ the complexity is increased by a factor of 5.46, whereas the complexity of obtaining the optimal NL for $V = 8$ is increased 6.46 times compared to $V = 7$. The scenario of $V = 10$ characterized in Fig. 23 and associated with different vertically stacked markers representing the $\aleph_{gen} = \{3, 6, 9, 12, 15, 18, 21\}$ generations incremented by 3 from bottom to the top corresponds to the line associated with the star marker at the top in Fig. 22, which commences from 40×10^4hrs of NL

with $\aleph_{gen} = 3$ and converges to 55×10^4hrs of near-optimal NL in conjunction with $\aleph_{gen} = 21$. Therefore, one can readily observe that the "Near-optimal NL" points are selected in Fig. 23 based on their convergence to the near-optimal NL values extracted from Fig. 22. For example, convergence to the optimal NL at $\aleph_{gen} = 21$ for the $V = 10$ scenario can be clearly seen from Fig. 22, which is explicitly marked as the "Near-optimal NL" point in Fig. 23 by a diamond-marker.

D. E2EB VERSUS SINR PERFORMANCE PER WSN
In this section, we provide the E2EB versus SINR performance analysis of the WSNs operated with the aid of uncoded BPSK and a 1/2-rate CC hard-decoded as well as soft-decoded QPSK scheme communicating over an AWGN channel. Fully connected WSNs consisting of $V = \{4, 10\}$ nodes for the SOGA are considered for various RSSs in Figs. 24a–24b, respectively. In all scenarios of SOGA, the E2EB is the lowest for 1/2-rate-CC soft-decoded QPSK at a given SINR value, which can be seen from Figs. 24a–24b. The E2EB of the system model considered slightly decreases upon increasing V, which is due to the higher chances of selecting a longer hop for the end-to-end transmission, yielding more accumulated bit errors during the passage of the message through to the DN. Furthermore, in most of the scenarios, especially for lower V values, RSS-LNOH performs slightly better in terms of its E2EB performance compared to the other RSSs. The main reason behind this is a natural consequence of using RSS-LNOH as a delay-aware scheme, which relies on the route having the lowest number of hops. Consequently, on the routes, where each link operates at the same SINR, less bit errors are accumulated over less hops. Another important point is that for a higher V, e.g. $V = 10$ the E2EB curves overlap in Fig. 24b, which means that the difference between the E2EB performances of the RSSs is barely noticeable. The fundamental reason behind this is that for a higher V having a larger number of distinct routes, the probability of requiring a RSS is low, because the chance of having only a single route associated with the maximum NL is extremely high. More explicitly, there may only be a single route having the maximum NL or routes having the same number of hops. Therefore, RSSs will always provide the same E2EB due to the selection of the specific route having the same number of hops in each RL iteration. Consequently, the E2EB performance will be similar, regardless of the RSSs. In Figs. 24a–24b, we note that ESA and SOGA perform identically within the measurement error of each other.

E. E2EB VERSUS SINR PERFORMANCE FOR RSS-LTED
Here, we consider the E2EB versus SINR performance analysis of various WSNs composed of V sensor nodes operating with the aid of uncoded BPSK, a 1/2-rate CC hard-decoded as well as soft-decoded QPSK MCSs communicating over an AWGN channel. Fully connected WSNs consisting of $V = \{4, 6, 8, 10\}$ nodes in the SOGA are considered for only RSS-LTED in Fig. 25. Explicitly, Fig. 25 illustrates the E2EB performance upon increasing the number of nodes.
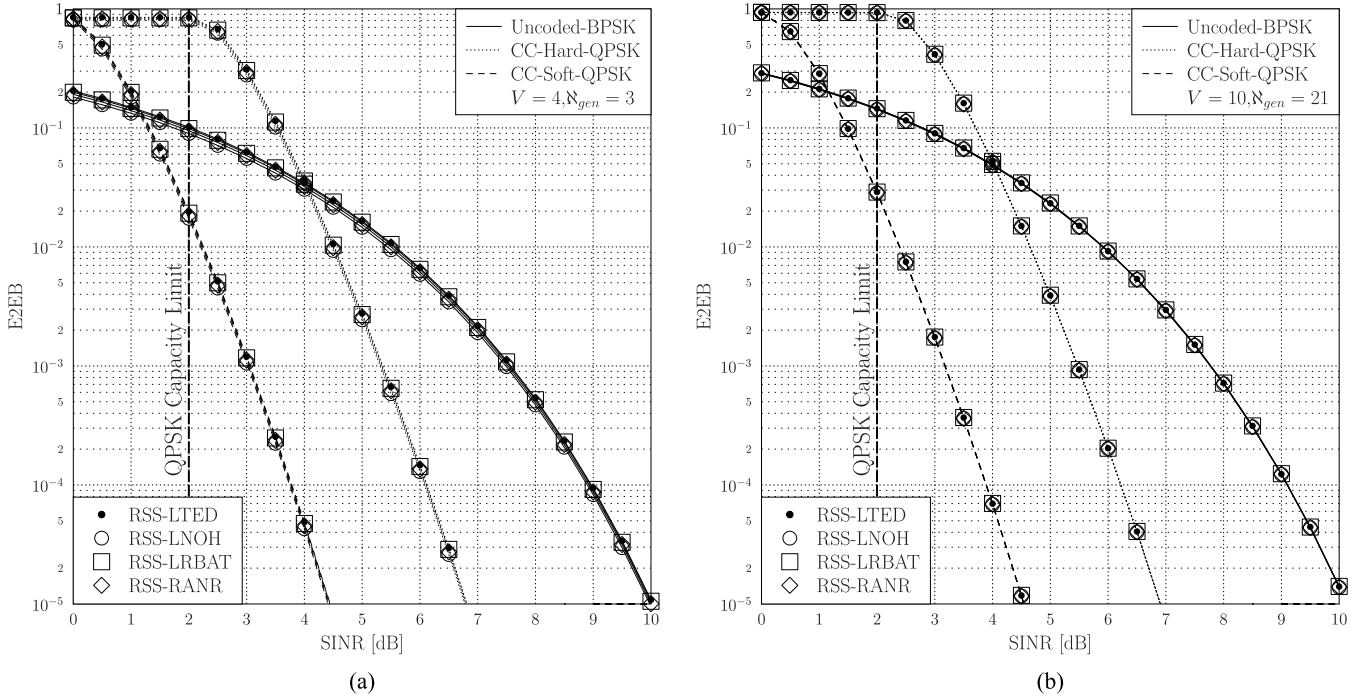
FIGURE 24. E2EB versus SINR performance of MCSs for each RSSs of SOGA using $\aleph_{gen}$ generations specifically chosen for the corresponding WSN having V nodes. (a) For $\aleph_{gen} = 3$ and $V = 4$. (b) For $\aleph_{gen} = 21$ and $V = 10$.

At the same SINR value, the highest E2EB belongs to the WSN composed of $V = 10$ nodes in the SOGA compared to the WSNs consisting of a lower number of nodes. One of the main reasons behind this is that the WSNs composed of larger number of nodes have a higher chance of achieving the maximum RL with the aid of the best route
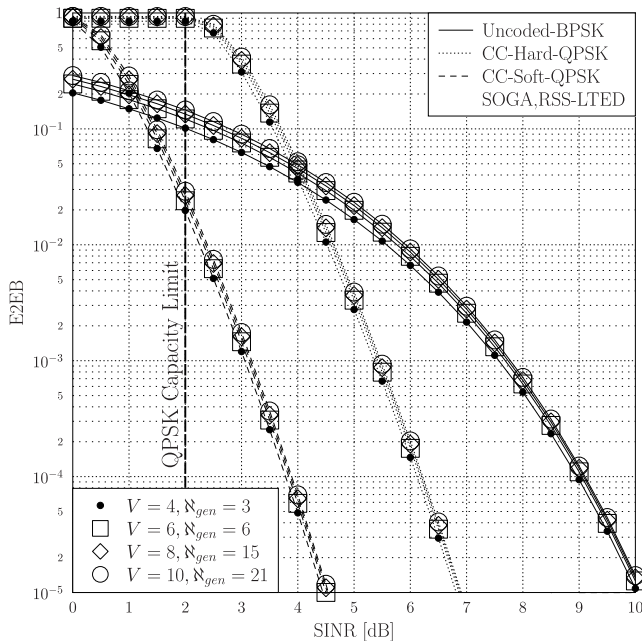

FIGURE 25. E2EB versus SINR performance of MCSs for each WSNs composed of V sensor nodes considering RSS-LTED in SOGA.

having longer hops in each iteration of the RL computation. The other main reason is that of relying on the worst-case E2EB computation strategy. We select the final route amongst the best routes obtained by each RL computation providing the longest hop. More explicitly, let us assume that the NL computation requires three iterations for RL computation. Then, each iteration provides us both with its best route and with the associated RL value, depending on the RSS. Once three iterations have been completed, the E2EB of these three best routes is calculated, respectively and the route that provides us with the worst E2EB value is selected, since we aim for finding the upper bound of the E2EB for the WSN considered. Here, the selection of the worst E2EB requires the selection of the route associated with the longest hop due to the specific nature of the E2EB computation. Therefore, the selection of the route having the worst-case E2EB requires longer hops, which in return yields higher E2EB for larger networks, as illustrated in Fig. 25. We note in the context of Fig. 25 that ESA and SOGA perform identically within the measurement error.

F. AVERAGE NL VERSUS E2EB PERFORMANCE PER WSN
The average NL versus E2EB trade-off is of salient importance, since it characterizes the QoS of the system model considered. In this section, we provide the average NL versus E2EB performance analysis of the WSNs operated with the aid of uncoded BPSK, a 1/2-rate CC hard-decoded as well as soft-decoded QPSK MCSs communicating over an AWGN channel. The fully connected WSNs composed of $V = \{4, 5, 6, 7\}$ nodes for the ESA and $V = 10$ nodes
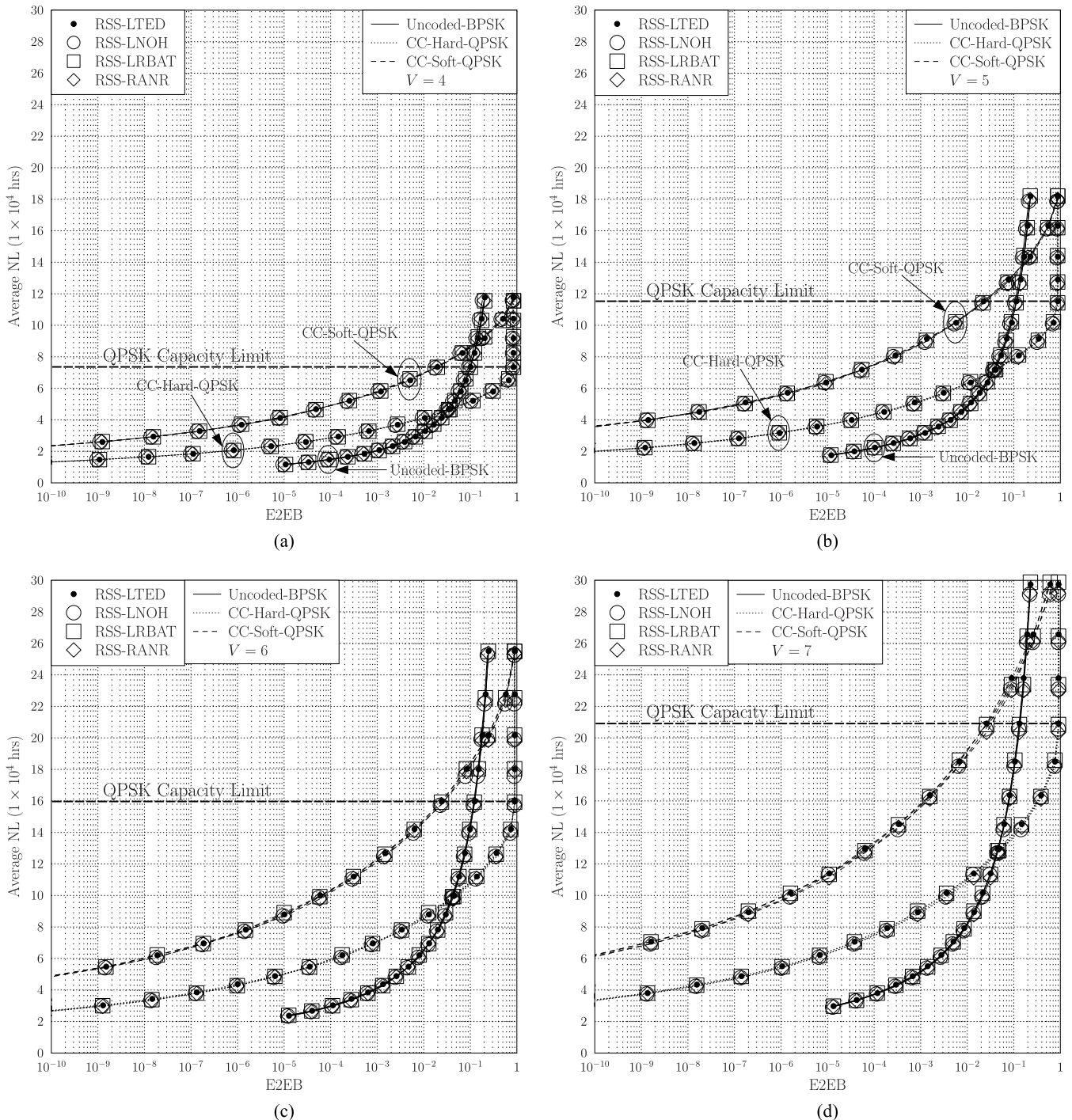
FIGURE 26. Average NL versus E2EB performance of MCSs for each RSSs of ESA in a fully connected WSN having *V* = {4, 5, 6, 7} nodes. (a) For *V* = 4. (b) For *V* = 5. (c) For *V* = 6. (d) For *V* = 7.

for the SOGA are considered for various RSSs in Figs. 26a–26d and Fig. 27, respectively. The E2EB performance of the 1/2-rate CC soft-decoded QPSK MCS is better than any of the other MCSs in all scenarios of both the ESA and the SOGA. For example, in the $V = 4$ scenario of ESA, at the same E2EB of 10^{-3}, approximately 4×10^4hrs of NL gain is achieved by the

1/2-rate CC soft-decoded QPSK MCS compared to uncoded BPSK and nearly 2.4×10^4hrs of NL gain compared to the 1/2-rate CC hard-decoded QPSK MCS. For an E2EB of 10^{-3}, the NL gain of 1/2-rate CC soft-decoded QPSK MCS for the $V = 5$ scenario is increased to approximately 6×10^4hrs compared to uncoded BPSK and to about 4×10^4hrs compared to 1/2-rate CC hard-decoded
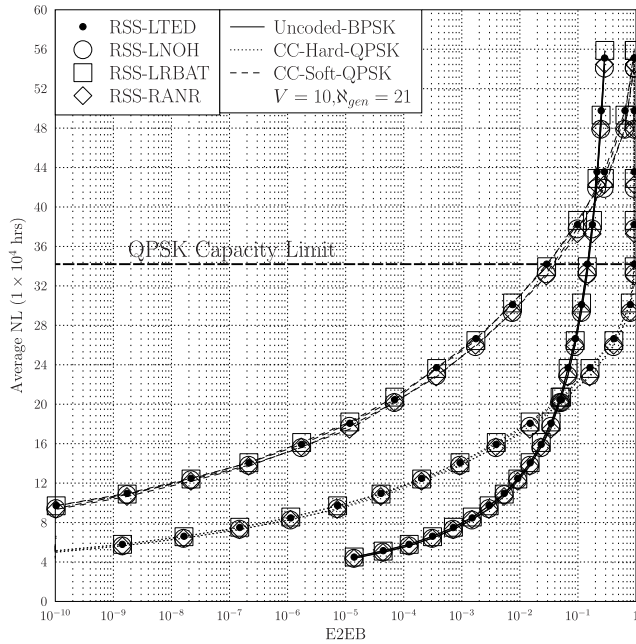
FIGURE 27. Average NL versus E2EB performance of MCSs for each RSSs of SOGA using $\aleph_{gen}$ generations specifically chosen for the corresponding WSN having $V = 10$ nodes.

QPSK MCS. The NL gain further increases upon introducing additional sensor nodes, namely for a $V = 6$ scenario approximately to 8×10^4hrs of NL compared to uncoded BPSK and to about 5×10^4hrs compared to 1/2-rate CC hard-decoded QPSK MCS. Similarly, for $V = 7$ this gain increases to about 10×10^4hrs of NL compared to uncoded BPSK and to about 7×10^4hrs of NL compared to the 1/2-rate CC hard-decoded QPSK MCS. Since the NL results converged to their optimal values under the SOGA, the E2EB performance of the ESA seen in Figs. 26a–26d and that of the SOGA recorded for the scenarios having the same number of nodes perform identically within the measurement error. Therefore, the E2EB performance analysis of ESA provided for $V = \{4, 5, 6, 7\}$ nodes is also carried out for the corresponding SOGA scenarios. Finally, for the $V = 10$

scenario of the SOGA, as illustrated in Fig. 27, a NL gain of 17×10^4hrs is attained compared to uncoded BPSK and 10×10^4hrs compared to 1/2-rate CC hard-decoded QPSK MCS at the same E2EB of 10^{-3}. Note that we were not able to generate the NL versus E2EB performance curves for $V = 10$ for the ESA due to its excessive computational complexity. We may conclude that the average NL versus E2EB trade-off for the various RSSs and MCSs in the considered fully connected WSNs composed of V sensor nodes provides the network designer with insights concerning the interplay between the NL and E2EB, depending on the application considered.

V. APPLICATION SCENARIOS

Our NL maximization approach significantly extends the lifetime of the WSN considered, compared to our previous studies in [14] and [15]. Therefore, our NL maximization approach is particularly well-suited for the applications that require longer network connectivity and operations in military battlefields, in monitoring climate changes and so on. For instance, the longevity of network operations in the military battlefield is crucial, since the hostile territory may become inaccessible and thus the battery of the sensors cannot be replaced. Therefore, a significant piece of information may be captured by a specific sensor and relaying its information to the base station is vital. More particularly, a specific sensor or a group of sensors that are located closer to the hostile targets may in fact carry the most significant information. Therefore, using these sensor(s) as the more significant sensor(s) and assuming that the rest of the sensors relay these significant pieces of information can conserve more energy and this can assist us in extending the NL, as described in our NL maximization technique.

Another example of densely deployed WSNs may be found in a football stadium, where each user carries a RFID sensor for health and safety reasons. Whenever a predefined threshold is exceeded, as exemplified by a high temperature, the information is relayed to the base station by hundreds of sensors. Again, only the most crucial information is transmitted

TABLE 13. The number of CFEs required for the convergence of the ESA and SOGA for different V values and for the RSS-LTED only.

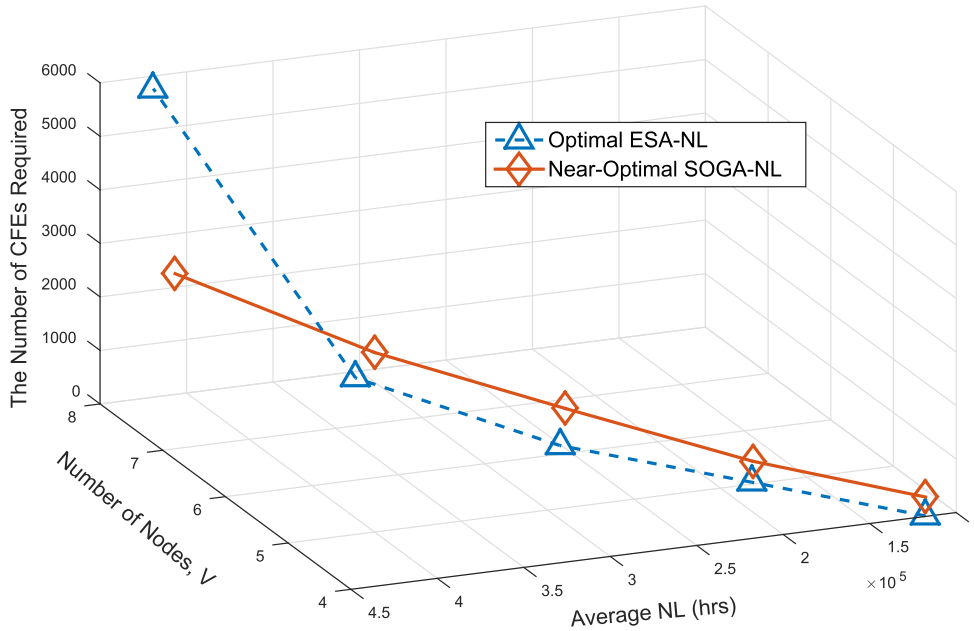| V	ESA-CFEs	SOGA-CFEs	Optimal ESA-NL [hrs]	Near-optimal SOGA-NL [hrs]
4	9.43	362.05	117, 682.52	117, 682.52
5	35.50	425.84	181, 886.36	181, 385.35
6	163.63	839.66	256, 745.29	253, 381.50
7	892.39	1, 328.11	338, 474.14	327, 753.47
8	5, 765.32	2, 256.23	419, 264.37	406, 622.97
10		3, 453.33		551, 086.69

FIGURE 28. Discrepancy from the ESA as a benchmark of the NL, upon increasing *V*.

to the base station by selecting the most lifetime-efficient route amongst thousands of potential alternative routes. Nonetheless, there are numerous other applications [3], [4] for the employment of our NL maximization framework, including environmental monitoring [56], surveillance [57], smart water quality monitoring, smart environment sensing, smart metering, smart agricultural applications, health monitoring and smart cities [58], just to name a few.

VI. SUMMARY AND CONCLUSIONS

In this paper, the NL maximization of interference-limited fully connected WSNs composed of *V* nodes associated with a single source and destination is considered, where the SN and the DN are located at the opposite corners of the sensor field of Fig. 11 to ascertain the longest distance between them, so that the system model guarantees the utilization of alternative routes for the end-to-end transmission. The information to be transmitted is only generated at the SN and the aim of the system model considered is to carry the SN's information to the DN via the relays, which are also capable of decoding and forwarding the information relayed. For the sake of mitigating the interference, we use the SPTS TDMA scheduling method, where on each route a node can only interfere with another node at the distance of *T*, if they are scheduled during the same TS. Moreover, each sensor node is equipped with a limited battery capacity and we only consider the transmit power as the main ED factor. Moreover, the E2EB constituting the worst-case BER of the fully connected WSN considered is formulated in (3) for uncoded BPSK, 1/2-rate CC hard-decoded and soft-decoded QPSK MCSs, as described in Section II-B. Naturally, the NL versus E2EB performance can be obtained for any arbitrary MCSs. In the system model described in Section II, we proposed the ESA

and the SOGA for solving the linear optimization problem formulated for each route given by (8)–(11) in Section III-A. Note that the ESA finds the optimal NL, where the best possible NL can be achieved by checking all the possible solution candidates of the entire solution search space, which the NL performance of the SOGA is benchmarked against. However, the SOGA is designed in a way that it can intelligently search through a limited fraction of the solution space using genetic operators. Since the NL is strictly dependent on the battery level of the SN, it is described in two stages; first stage is responsible for the computation of the RL, until the SN fully drains its battery, because the system model is only subjected to the end-to-end transmission of the information generated at the SN with the aid of the maximum-RL-aware routes. The second stage is involved in the accumulation of RLs during the iterations of the RL computation, until the SN battery is fully depleted. Thus, the NL computation may consist of a few RL computation iterations, where in each iteration the best route is selected from the set of routes having the maximum RL for end-to-end transmission. This selection process may rely on several criteria, which are described as the set of RSSs methods constituted by the RSS-LTED, RSS-LNOH, RSS-LRBAT, RSS-RANR of Section III-B2.

The computation of the NL in such networks may be challenging due to its computational complexity for a large *V*, which might result in numerous alternative routes that have to be evaluated in terms of their RL. Moreover, considering the exponential increase of the number of distinct routes upon increasing the number of nodes, an algorithm associated with a much reduced complexity is required for NL maximization. Therefore, the SOGA of Section III-B5 was introduced for circumventing the shortcomings of the ESA for larger network sizes. Upon using the parameter values of Table 12

discussed in Section IV, an approximately 45,000hrs of NL gain is attained for the WSN considered, when operating at SINR = 2dB by inserting an additional sensor node into a WSN having an arbitrary size. This NL gain is reduced to about 5,500hrs, when the WSN operates at SINR = 10dB. We also observed that for $V \leq 7$ using the ESA is a better option due to its lower computational complexity at a specific target-performance. Observe from Table 13 that for $V = 7$ the computational complexity of the ESA and SOGA is similar. As illustrated in Fig. 28, the NL discrepancy of the SOGA with respect to the optimal NL value of the ESA is as low as 3.17%, which corresponds to 1.07×10^4hrs of NL. We say that the NL is converged to its optimal NL value, if the NL discrepancy is less than 3.5%. For example, in the $V = 8$ scenario the NL gap of the SOGA with respect to the upper bound ESA is 3.02%. Hence, in the $V = 8$ scenario of Fig. 19 the NL computed by the SOGA becomes near-optimal at a 2.56 times lower complexity compared to the ESA. Nonetheless, observe in Fig. 23 that the SOGA imposed a lower complexity than the ESA for any WSN having $V > 7$. For convenience, Table 13 summarizes the computational complexity of both the ESA and SOGA imposed for different V values, when relying on the RSS-LTED. Again, the convergence of SOGA to a near-optimal NL value is achieved at a much reduced complexity.

Furthermore, observe in Figs. 20 and 21 that both RSS-LTED and RSS-LRBAT have a higher NL owing to their energy-awareness compared to the other RSSs. Additionally, as illustrated in Figs. 24a–24d, RSS-LNOH tends to exhibit a better E2EB performance than the other RSSs due to its delay-awareness, which naturally results in the accumulation of less bit errors as a benefit of selecting the route having the least number of hops. However, one can conclude that since the objective function is formulated for achieving RL maximization, the RSSs presented attain a similar NL. More explicitly, as long as the RL is maximized, any route associated with the maximum RL amongst the routes having the same maximum RL can be selected for the end-to-end transmission. On the other hand, the decision concerning the route selection significantly affects the E2EB performance, since the computation of the E2EB strictly relies on the number of hops and the MCSs considered.

Nonetheless, the 1/2-rate CC soft-decoded QPSK MCS outperforms the other MCSs in all scenarios for the ESA and SOGA. For example, in the $V = 4$ scenario of the ESA, at the same E2EB of 10^{-3} the 1/2-rate CC soft-decoded QPSK MCS achieves an approximately 4×10^4hrs of NL gain compared to uncoded BPSK and nearly 2.4×10^4hrs of NL gain compared to the 1/2-rate CC hard-decoded QPSK MCS. This gain is further increased upon increasing the number of nodes. Moreover, WSNs composed of larger number of nodes result in higher E2EB. The main reason for this is that the route selection strategy associated with the worst-case E2EB requires longer hops, which in return yields a higher E2EB for larger networks. Another reason is that WSNs composed of larger number of nodes have a higher chance of achieving

the maximum RL with the aid of the best route having longer hops in each iteration of the RL computation.

REFERENCES

[1] I. F. Akyildiz, W. Su, Y. Sankarasubramaniam, and E. Cayirci, "A survey on sensor networks," *IEEE Commun. Mag.*, vol. 40, no. 8, pp. 102–114, Aug. 2002.

[2] I. F. Akyildiz, W. Su, Y. Sankarasubramaniam, and E. Cayirci, "Wireless sensor networks: A survey," *Comput. Netw.*, vol. 38, no. 4, pp. 393–422, Mar. 2002.

[3] K. Romer and F. Mattern, "The design space of wireless sensor networks," *IEEE Wireless Commun.*, vol. 11, no. 6, pp. 54–61, Dec. 2004.

[4] D. Puccinelli and M. Haenggi, "Wireless sensor networks: Applications and challenges of ubiquitous sensing," *IEEE Circuits Syst. Mag.*, vol. 5, no. 3, pp. 19–31, Sep. 2005.

[5] V. C. Gungor and G. P. Hancke, "Industrial wireless sensor networks: Challenges, design principles, and technical approaches," *IEEE Trans. Ind. Electron.*, vol. 56, no. 10, pp. 4258–4265, Oct. 2009.

[6] Y. Chen and Q. Zhao, "An integrated approach to energy-aware medium access for wireless sensor networks," *IEEE Trans. Signal Process.*, vol. 55, no. 7, pp. 3429–3444, Jul. 2007.

[7] K. Cohen and A. Leshem, "A time-varying opportunistic approach to lifetime maximization of wireless sensor networks," *IEEE Trans. Signal Process.*, vol. 58, no. 10, pp. 5307–5319, Oct. 2010.

[8] W. Xu, Q. Shi, X. Wei, Z. Ma, X. Zhu, and Y. Wang, "Distributed optimal rate–reliability–lifetime tradeoff in time-varying wireless sensor networks," *IEEE Trans. Wireless Commun.*, vol. 13, no. 9, pp. 4836–4847, Sep. 2014.

[9] R. Madan and S. Lall, "Distributed algorithms for maximum lifetime routing in wireless sensor networks," *IEEE Trans. Wireless Commun.*, vol. 5, no. 8, pp. 2185–2193, Aug. 2006.

[10] M. Cheng, X. Gong, and L. Cai, "Joint routing and link rate allocation under bandwidth and energy constraints in sensor networks," *IEEE Trans. Wireless Commun.*, vol. 8, no. 7, pp. 3770–3779, Jul. 2009.

[11] H. Wang, N. Agoulmine, M. Ma, and Y. Jin, "Network lifetime optimization in wireless sensor networks," *IEEE J. Sel. Areas Commun.*, vol. 28, no. 7, pp. 1127–1137, Sep. 2010.

[12] A. A. Aziz, Y. A. Sekercioglu, P. Fitzpatrick, and M. Ivanovich, "A survey on distributed topology control techniques for extending the lifetime of battery powered wireless sensor networks," *IEEE Commun. Surveys Tuts.*, vol. 15, no. 1, pp. 121–144, Feb. 2013.

[13] R. Madan, S. Cui, S. Lall, and A. Goldsmith, "Cross-layer design for lifetime maximization in interference-limited wireless sensor networks," *IEEE Trans. Wireless Commun.*, vol. 5, no. 11, pp. 3142–3152, Nov. 2006.

[14] H. Yetgin, K. T. K. Cheung, M. El-Hajjar, and L. Hanzo, "Cross-layer network lifetime maximization in interference-limited WSNs," *IEEE Trans. Veh. Technol.*, vol. 64, no. 8, pp. 3795–3803, Aug. 2015.

[15] H. Yetgin, K. T. K. Cheung, M. El-Hajjar, and L. Hanzo, "Cross-layer network lifetime optimisation considering transmit and signal processing power in wireless sensor networks," *IET Wireless Sensor Syst.*, vol. 4, no. 4, pp. 176–182, Dec. 2014.

[16] H. Yetgin, K. T. K. Cheung, and L. Hanzo, "Multi-objective routing optimization using evolutionary algorithms," in *Proc. IEEE Wireless Commun. Netw. Conf. (WCNC)*, Paris, France, Apr. 2012, pp. 3030–3034.

[17] D. Alanis, P. Botsinis, S. X. Ng, and L. Hanzo, "Quantum-assisted routing optimization for self-organizing networks," *IEEE Access*, vol. 2, pp. 614–632, 2014.

[18] R. Madan, S. Cui, S. Lall, and A. J. Goldsmith, "Modeling and optimization of transmission schemes in energy-constrained wireless sensor networks," *IEEE/ACM Trans. Netw.*, vol. 15, no. 6, pp. 1359–1372, Dec. 2007.

[19] J. Long, M. Dong, K. Ota, A. Liu, and S. Hai, "Reliability guaranteed efficient data gathering in wireless sensor networks," *IEEE Access*, vol. 3, pp. 430–444, May 2015.

[20] L. Lin, X. Lin, and N. B. Shroff, "Low-complexity and distributed energy minimization in multi-hop wireless networks," in *Proc. IEEE Int. Conf. Comput. Commun. (INFOCOM)*, Anchorage, AK, USA, May 2007, pp. 1685–1693.

[21] Q. Dong, "Maximizing system lifetime in wireless sensor networks," in *Proc. 4th Int. Symp. Inf. Process. Sensor Netw. (IPSN)*, Apr. 2005, pp. 13–19.

[22] L. Badia, A. Botta, and L. Lenzini, "A genetic approach to joint routing and link scheduling for wireless mesh networks," *Ad Hoc Netw.*, vol. 7, no. 4, pp. 654–664, Jun. 2009.

[23] J. Jia, X. Wang, and J. Chen, "A genetic approach on cross-layer optimization for cognitive radio wireless mesh network under SINR model," *Ad Hoc Netw.*, vol. 27, pp. 57–67, Apr. 2015.

[24] A. Azari and G. Miao, "Lifetime-aware scheduling and power control for M2M communications in LTE networks," in *Proc. IEEE Veh. Technol. Conf. (VTC)*, Glasgow, Scotland, May 2015, pp. 1–5.

[25] A. Azari and G. Miao, "Lifetime-aware scheduling and power control for cellular-based M2M communications," in *Proc. IEEE Wireless Commun. Netw. Conf. (WCNC)*, New Orleans, LA, USA, Mar. 2015, pp. 1171–1176.

[26] H. Kwon, T. H. Kim, S. Choi, and B. G. Lee, "Lifetime maximization under reliability constraint via cross-layer strategy in wireless sensor networks," in *Proc. IEEE Wireless Commun. Netw. Conf.*, vol. 3. Mar. 2005, pp. 1891–1896.

[27] H. Kwon, T. H. Kim, S. Choi, and B. G. Lee, "Cross-layer lifetime maximization under reliability and stability constraints in wireless sensor networks," in *Proc. IEEE Int. Conf. Commun. (ICC)*, vol. 5. Seoul, Korea, May 2005, pp. 3285–3289.

[28] H. Kwon, T. H. Kim, S. Choi, and B. G. Lee, "A cross-layer strategy for energy-efficient reliable delivery in wireless sensor networks," *IEEE Trans. Wireless Commun.*, vol. 5, no. 12, pp. 3689–3699, Dec. 2006.

[29] Y. Cui, Y. Xue, and K. Nahrstedt, "A utility-based distributed maximum lifetime routing algorithm for wireless networks," *IEEE Trans. Veh. Technol.*, vol. 55, no. 3, pp. 797–805, May 2006.

[30] C. Zhu, S. Wu, G. Han, L. Shu, and H. Wu, "A tree-cluster-based data-gathering algorithm for industrial WSNs with a mobile sink," *IEEE Access*, vol. 3, pp. 381–396, May 2015.

[31] R. Khanna, H. Liu, and H.-H. Chen, "Dynamic optimization of secure mobile sensor networks: A genetic algorithm," in *Proc. IEEE Int. Conf. Commun. (ICC)*, Glasgow, Scotland, Jun. 2007, pp. 3413–3418.

[32] C. Hua and T. P. Yum, "Optimal routing and data aggregation for maximizing lifetime of wireless sensor networks," *IEEE/ACM Trans. Netw.*, vol. 16, no. 4, pp. 892–903, Aug. 2008.

[33] Y. Gu, M. Pan, and W. W. Li, "Prolonging the lifetime of large scale wireless sensor networks via base station placement," in *Proc. IEEE Veh. Technol. Conf. (VTC)*, Las Vegas, NV, USA, Sep. 2013, pp. 1–5.

[34] H. Chenji and R. Stoleru, "Pareto optimal cross layer lifetime optimization for disaster response networks," in *Proc. Int. Conf. Commun. Syst. Netw. (COMSNETS)*, Bengaluru, India, Jan. 2014, pp. 1–8.

[35] Y. Shi, Y. E. Sagduyu, and J. H. Li, "Low complexity multi-layer optimization for multi-hop wireless networks," in *Proc. Military Commun. Conf. (MILCOM)*, Oct./Nov. 2012, pp. 1–6.

[36] J.-H. Chang and L. Tassiulas, "Maximum lifetime routing in wireless sensor networks," *IEEE/ACM Trans. Netw.*, vol. 12, no. 4, pp. 609–619, Aug. 2004.

[37] A. Behzadan, A. Anpalagan, and B. Ma, "Prolonging network lifetime via nodal energy balancing in heterogeneous wireless sensor networks," in *Proc. IEEE Int. Conf. Commun. (ICC)*, Kyoto, Japan, Jun. 2011, pp. 1–5.

[38] J. Long, M. Dong, K. Ota, and A. Liu, "Achieving source location privacy and network lifetime maximization through tree-based diversionary routing in wireless sensor networks," *IEEE Access*, vol. 2, pp. 633–651, Jul. 2014.

[39] A. B. M. Alim Al Islam, M. S. Hossain, V. Raghunathan, and Y. C. Hu, "Backpacking: Energy-efficient deployment of heterogeneous radios in multi-radio high-data-rate wireless sensor networks," *IEEE Access*, vol. 2, pp. 1281–1306, Nov. 2014.

[40] A. Goldsmith, *Wireless Communications*. Cambridge, U.K.: Cambridge Univ. Press, 2005.

[41] O. K. Tonguz and G. Ferrari, *Ad Hoc Wireless Networks: A Communication-Theoretic Perspective*. New York, NY, USA: Wiley, 2006.

[42] O. K. Tonguz and G. Ferrari, "A communication-theoretic approach to ad hoc wireless networking," in *Proc. 3rd Annu. IEEE Commun. Soc. Sensor Ad Hoc Commun. Netw. (SECON)*, vol. 2. Reston, VA, USA, Sep. 2006, pp. 715–722.

[43] Y. Chen and Q. Zhao, "On the lifetime of wireless sensor networks," *IEEE Commun. Lett.*, vol. 9, no. 11, pp. 976–978, Nov. 2005.

[44] J. Li and G. AlRegib, "Function-based network lifetime for estimation in wireless sensor networks," *IEEE Signal Process. Lett.*, vol. 15, pp. 533–536, Jul. 2008.

[45] J. W. Jung and M. A. Weitnauer, "On using cooperative routing for lifetime optimization of multi-hop wireless sensor networks: Analysis and guidelines," *IEEE Trans. Commun.*, vol. 61, no. 8, pp. 3413–3423, Aug. 2013.

[46] I. Dietrich and F. Dressler, "On the lifetime of wireless sensor networks," *ACM Trans. Sensor Netw.*, vol. 5, no. 1, pp. 1–39, Feb. 2009.

[47] S. Boyd and L. Vandenberghe, *Convex Optimization*. Cambridge, U.K.: Cambridge Univ. Press, 2004.

[48] *IBM's ILOG CPLEX Optimization Studio*. [Online]. Available: http://www-01.ibm.com/support/knowledgecenter/SSSA5P/welcome, accessed Nov. 5, 2015.

[49] S. Savazzi, L. Goratti, U. Spagnolin, and M. Latva-Aho, "Short-range wireless sensor networks for high density seismic monitoring," in *Proc. Wireless World Res. Forum*, Paris, France, May 2009, pp. 1–5.

[50] J. G. Proakis, *Digital Communications*. New York, NY, USA: McGraw-Hill, 2001.

[51] K. Deb, A. Pratap, S. Agarwal, and T. Meyarivan, "A fast and elitist multiobjective genetic algorithm: NSGA-II," *IEEE Trans. Evol. Comput.*, vol. 6, no. 2, pp. 182–197, Apr. 2002.

[52] C. W. Ahn and R. S. Ramakrishna, "A genetic algorithm for shortest path routing problem and the sizing of populations," *IEEE Trans. Evol. Comput.*, vol. 6, no. 6, pp. 566–579, Dec. 2002.

[53] S. S. Iyengar, H.-C. Wu, N. Balakrishnan, and S. Y. Chang, "Biologically inspired cooperative routing for wireless mobile sensor networks," *IEEE Syst. J.*, vol. 1, no. 1, pp. 29–37, Sep. 2007.

[54] *IEEE Standard for Information Technology—Local and Metropolitan Area Networks—Specific Requirements—Part 15.4: Wireless Medium Access Control (MAC) and Physical Layer (PHY) Specifications for Low Rate Wireless Personal Area Networks (WPANs)*, Standard, Sep. 2006.

[55] M. Albulet, *RF Power Amplifiers*. Raleigh, NC, USA: SciTech, 2001.

[56] K. Martinez, J. K. Hart, and R. Ong, "Environmental sensor networks," *Computer*, vol. 37, no. 8, pp. 50–56, Aug. 2004.

[57] Y. Ye, S. Ci, A. K. Katsaggelos, Y. Liu, and Y. Qian, "Wireless video surveillance: A survey," *IEEE Access*, vol. 1, pp. 646–660, Sep. 2013.

[58] S. Djahel, R. Doolan, G.-M. Muntean, and J. Murphy, "A communications-oriented perspective on traffic management systems for smart cities: Challenges and innovative approaches," *IEEE Commun. Surveys Tuts.*, vol. 17, no. 1, pp. 125–151, Mar. 2015.

HALIL YETGIN (S'11) received the B.Eng. degree in computer engineering from Selcuk University, Konya, Turkey, in 2008, and the M.Sc. degree in wireless communications from the University of Southampton, Southampton, U.K., in 2010, where he is currently pursuing the Ph.D. degree in wireless communications with the Southampton Wireless Research Group. Then, he was a Software Engineer with Gulhane Military Medical Academy, Ankara, Turkey, in 2009. He was a recipient of the full scholarship granted by the Ministry of National Education, Turkey.

His research interests include energy-efficient cross-layer design, network lifetime maximization, multiobjective routing optimization, and resource allocation algorithm design in wireless networks.

KENT TSZ KAN CHEUNG (S'09) received the B.Eng. (Hons.) degree in electronic engineering and the Ph.D. degree in wireless communications from the University of Southampton, Southampton, U.K., in 2009 and 2015, respectively. He was a recipient of the EPSRC Industrial CASE Award in 2009, and was involved with the Core 5 Green Radio Project of the Virtual Centre of Excellence in Mobile and Personal Communications.

His research interests include energy-efficiency, multicarrier multiple-input multiple- output communications, cooperative communications, resource allocation, and optimization.

MOHAMMED EL-HAJJAR (M'05) received the B.Eng degree in electrical engineering from the American University of Beirut, Beirut, Lebanon, in 2004, and the M.Sc. degree in radio-frequency communication systems and the Ph.D. degree in wireless communications from the University of Southampton, Southampton, U.K., in 2005 and 2008, respectively.

He joined Imagination Technologies as a Design Engineer, where he was involved in designing and developing imagination's multistandard communications platform, which resulted in three patents. Since 2012, he has been a Lecturer with the Wireless Group, School of Electronics and Computer Science, University of Southampton, Southampton, U.K. He has authored a Wiley–IEEE book and in excess of 50 journal and international conference papers. His research interests include the development of intelligent communications systems, in particular, energy-efficient transceiver design, cross-layer optimization for large-scale networks, multiple-input multiple-output systems, millimeter-wave communications, and radio-over-fiber systems.

Dr. El-Hajjar received several academic awards, including the Dean's Award for Creative Achievement, the Dorothy Hodgkin Postgraduate Award, and the 2010 IEEE International Conference on Communications Best Paper Award.

LAJOS HANZO (M'91–SM'92–F'03) received the D.Sc. degree in electronics in 1976 and the Ph.D. degree in 1983. During his 35-year career in telecommunications, he has held various research and academic posts in Hungary, Germany, and U.K. Since 1986, he has been with the School of Electronics and Computer Science, University of Southampton, U.K., where he holds the Chair in telecommunications. He has successfully supervised 80 Ph.D. students, has co-authored 20 John Wiley/IEEE Press books on mobile radio communications totaling in excess of 10 000 pages, has authored 1500+ research entries at IEEE Xplore, acted both as the TPC and General Chair of the IEEE conferences, presented keynote lectures, and has been awarded a number of distinctions. His research is funded by the European Research Council's Senior Research Fellow Grant. He is a fellow of the Royal Academy of Engineering, the Institute of Engineering and Technology, and the European Association for Signal Processing. In 2009, he received the honorary doctorate Doctor Honoris Causa by the Technical University of Budapest. He is currently directing a 60-strong academic research team, working on a range of research projects in the field of wireless multimedia communications sponsored by industry, the U.K. Engineering and Physical Sciences Research Council, the European IST Programme, and the Mobile Virtual Centre of Excellence, U.K. He is an enthusiastic supporter of industrial and academic liaison and he offers a range of industrial courses. He is also a Governor of the IEEE Vehicular Technology Society. From 2008 to 2012, he was the Editor-in-Chief of the IEEE Press and a Chair Professor at Tsinghua University, Beijing.

● ● ●